Hybrid Genome Sequence of *Cryptococcus neoformans* of Indian origin and Comparative Genome Analysis

Jananishree Sathiyamoorthy[1] and Jayapradha Ramakrishnan[*]

First Author: **Jananishree Sathiyamoorthy[1]**

Actinomycetes Bioprospecting Lab
Centre for Research in Infectious Diseases (CRID),
School of Chemical and Biotechnology, SASTRA Deemed University,
Tirumalaisamudram, Thanjavur – 613401, Tamilnadu, India.
Email: jananishreegsm96@gmail.com

Corresponding Author: **Jayapradha Ramakrishnan[*]**

Actinomycetes Bioprospecting Lab

Centre for Research in Infectious Diseases (CRID),

School of Chemical and Biotechnology, SASTRA Deemed University,

Tirumalaisamudram, Thanjavur – 613401, Tamilnadu, India.

Email: kavijayashal@gmail.com; antibioticbiology@gmail.com

Ph: +91-9952538211

Abstract

Objectives

The Indian isolate of *Cryptococcus neoformans* underwent complete genome sequencing to elucidate its genomic architecture and functional characteristics. Furthermore, this study aimed to comprehensively characterize the virulence factors (virulome), antibiotic resistance genes (resistome), and the pan-genome of *C. neoformans* spp. through a comparative genomic analysis, providing insights into the genetic diversity and evolutionary relationships among strains.

Methods

The genomic data of a clinical strain of *C. neoformans* was assembled and annotated by MaSuRCA5 and Braker tool. Along with this, the assembled genomic data of the 11 strains were retrieved from NCBI datasets. The comparative virulome, resistome, phylogeny and of the 12 *C. neoformans* genomes were analyzed using DFVF, AFRbase, BLAST, CLUSTAL Omega, MEGAX, and Orthovenn3, respectively.

Results

The sequenced isolate was identified as a member of the *Cryptococcus neoformans* var. *grubii* subspecies. Notably, virulence-related genes comprise approximately 4.8% of the total genome. A comparative genomic analysis of 12 study genomes revealed variations in virulence patterns, including differences in melanization, immune evasion, blood-brain barrier evasion, transcriptional regulation, and oxidative stress response. The phylogenetic study using MLST and orthologous clusters categorized the subspecies *grubii* and *neoformans* in different clades. Pan-genome analysis showed that 73.6% of orthologous gene clusters and 77.72% of orthologous proteins were conserved across all 12 study genomes, indicating a shared core genome. Furthermore, the evolutionary relatedness study of the pan-genome revealed gene expansion and contraction events among the study strains.

Conclusion

This pioneering study presents the first comprehensive genomic and comparative genomic analysis of *Cryptococcus* sp., incorporating data on virulence genes, antibiotic resistance, and pan-genome dynamics. Key findings reveal that strains Cn, H99, and JEC21 harbor crucial virulence genes associated with infection severity. While all study strains possess genes promoting antifungal resistance (AFR), most lack specific single nucleotide

polymorphisms defining AFR. Consistent with pan-genome analysis, our results show significant gene expansion and contraction events in these strains. This study underscores the importance of bioinformatic tools for efficient whole-genome analysis and large-scale comparative genomics research.

Keywords: *Cryptococcus neoformans* sp., Comparative genomics, Phylogeny, Virulome, Resistome, Pan-genome

1. Introduction

Cryptococcus sp. is a dimorphic environmental fungus that majorly infects HIV patients [1]. It is considered intricate because it is classified into two broad species, *C. neoformans* and *C. gatti*. Furthermore, two subspecies, *C. neoformans* var. *grubii* (serotype A) and *C. neoformans var. neoformans* (serotype D) were found. *C. gatti* was classified into serotype B and serotype C. Currently, there are nine major molecular types [2]. Among these, serotype A (*C. neoformans var. grubii*) is highly pathogenic and the molecular types VNI and VNII are widespread in the Indian population [3]. *C. neoformans* is considered one of the critical priority pathogens by WHO [4]. The high pathogenicity of serotype A is due to its escalated virulence factors, environmental adaptability, and immune evasion capabilities [5,6].

This ubiquitous pathogen frequently inhabits avian environments (pigeon droppings, claws and wings of pigeons), marshy areas, and decaying wood [7,8]. The infection begins in the lungs through the inhalation of cryptococcal spores/ infectious propagules. Once *Cryptococcus* colonizes the lungs it breaches the lungs and circulates to the liver, kidney and bone marrow through the bloodstream and disseminates to the brain via paracytosis, transcytosis and trojan horse mechanism [9,10]. The *Cryptococcus* sp. exhibits neurotropism owing to the presence of proteinases and urease that allow them to penetrate the blood-brain barrier (degradation of ECM components of the host) and survive. Tropical, subtropical and temperate locations have been found to have higher incidences of cryptococcal infection [11]. The prevalence of cryptococcal infection was high majorly in Sub-Saharan Africa (incidence: 6-10% among individuals with advanced HIV disease; mortality: 24% to 47% at 10 weeks post-diagnosis), followed by Asia and Pacific (incidence: 1 to 3% among the HIV infected individuals) [12]. These areas are influenced by a combination of environmental, ecological, socioeconomic, and healthcare-related

factors. It was estimated that 1, 52, 000 new cases and 1, 12, 000 (19%) deaths were reported globally each year. The advent of HAART reduced the incidence of cryptococcal infection but the mortality rate remains high [12].

In the recent decade, it was noted that immune-competent individuals are also acquiring the infection and the reason could be the result of the organism's increased pathogenicity, which could be caused by virulence, stress tolerance, or Anti-Fungal Resistance (AFR) [9]. The virulence factors of *Cryptococcus* sp. are the capsular polysaccharides (glucoronoxylomannan, galactoxylomannan), melanin, mannoproteins and certain lytic enzymes (urease, phospholipase and proteases) [13,14].

The preliminary role of the stress tolerance genes was to overcome the environmental stressors (temperature, pH, reactive oxygen species, reactive nitrogen species and nutrient starvation). In addition, the autophagy genes (also stress-tolerant genes) in *Cryptococcus* sp., play a role in cell differentiation, cell growth, morphology and pathogenesis. These ATGs play a critical role in bilateral reproduction [15–17]. The recent insights of cryptococcal genomics reveal that stress-tolerant genes play a pivotal role in modulating the major virulence factors synthesis and promoting AFR [18]. They also regulate the genes responsible for maintaining the cell wall, cell membrane integrity and also regulate the evasion of host immune response.

The development of AFR or tolerance, which is brought about by stable and heritable point mutations that impact the target and drug interaction is significantly influenced by the organism’s genetic background [19]. Complete Genome Sequencing (CGS) has revolutionized the understanding of AFR in *C. neoformans.* Though the inherent resistance (echinocandins resistance) is more common in *Cryptococcus* sp. the fungal genomics highlights the insights of acquired resistant mechanisms (target protein modification, over-expression of target proteins, and upregulation of multi-drug transporters) caused by genetic mutations and structural variations[19–21]. The mutation's non-primary target proteins also produce resistance to antifungal drugs [22].

In the earlier decades, PCR-Restriction Fragment Length Polymorphism and PCR fingerprinting were used to study *Cryptococcus* molecular epidemiology, the genetic structure of the fungus and genome plasticity. The recent advent and advancements in WGS help in

understanding the epidemiology and genetic structure of *Cryptococcus* sp.[23]. Globally the studies based on the WGS have demonstrated small genetic variability and a small number of chromosomal rearrangements across the molecular types and also the variations in gene content and structural changes due to translocations, aneuploidy and inversions were noted in *C. neoformans*. The WGS also helps in revealing the hybrids present between the *Cryptococcus* sp., complex [23]. In addition, WGS helps in identifying the microevolution signals of infecting strains revealing the rapid adaptation of the organism through hypermutation to identify genes related to the adaptation of an organism to the stress condition that include virulence and pathogenicity features and monitoring of outbreaks [23,24].

Considering it as a critical priority pathogen as described in the guidelines by WHO and the gap in the knowledge about the genomic features of clinical *Cryptococcus* species of Indian origin, this was the first study in India we demonstrated hybrid sequencing of *Cryptococcus neoformans* (clinical strain) and unravel the genomic aspects and comparative pan-genome analyses were made with the clinical isolates and an environmental isolate from NCBI datasets to understand the evolutionary relationships, resistome and virulome. To the best of our knowledge, this is the first kind of study to perform the hybrid sequence of the *Cryptococcus* genome, its resistome, virulome and pan-genome analysis.

2. Materials and Methods

2.1. Culture Isolation and DNA extraction

The comprehensive methodology is depicted in Figure 1. The *Cryptococcus* sp. (Cn) was collected from the microbiology lab of Trichy Medical College, Tamil Nadu, India sourced from the cryptococcal meningitis patient. The presumptive identification was performed by Indian ink staining after growing the yeast colonies in potato dextrose agar containing streptomycin. The purified yeast colonies were stored in 30% glycerol at -80°C.

Initially, the clinical isolate Cn was grown in Potato Dextrose Broth (PDB) and incubated for 48 hours at 37°C. Approximately 10^7 log phase cells were obtained by centrifugation at 7500 rpm for 10 minutes following the scheduled incubation period. The isopropanol precipitation technique, phenol-chloroform, and urea lysis buffer were used to extract the DNA from the

pellet. After two cycles of mechanical lysis, one cycle was finished with one milliliter of urea lysis buffer and four hours of incubation at 30°C. Proteinase K (0.02 ml) and Sarkosyl lysis buffer (0.4 ml) were added to the lysate, and the mixture was incubated for 1 hour at 55°C. After a three-minute break on ice and another three minutes of mechanical lysis at 2500 rpm, the cycle was repeated three times. RNase A was added to the lysate, and it was then incubated for 20 minutes at 65°C. The lysate was blended with an equal volume of phenol-chloroform, inverted, and centrifuged for 10 minutes at 4°C and 13,200 rpm. After transferring the aqueous phase to a fresh microcentrifuge tube and adding an equivalent volume of chloroform, isoamyl alcohol was added and the tube was centrifuged. After transferring the aqueous phase to a fresh microcentrifuge tube, DNA was precipitated in an equivalent volume of isopropanol. The pellet was washed with 70% ethanol, air dried and dissolved in 10mM Tris-Cl (pH 8.0).

The concentration and purity of genomic DNA were quantified using a Nanodrop Spectrophotometer (Thermo Scientific; 2000). DNA integrity was observed on agarose gel electrophoresis (supplementary figure 1). DNA concentration quantified using Qubit dsDNA HS assay kit.

2.2. Complete Genome Sequencing

2.2.1 Illumina library preparation, sequencing and preprocessing

The library preparation was performed with 50ng of quantified DNA. The QIASeq FX DNA Library Kit was used to prepare the library according to the protocol provided in the kit manual[25]. Indexing PCR was performed on the library to enrich the adapter-tagged fragments and purification of the amplified library was performed with High Prep TM beads. The library was quantified using a Qubit fluorometer (Thermo Fisher Scientific, MA, USA), and the Agilent 2200 Tape Station was used to evaluate the fragment size distribution of the library (supplementary figure 2).

The libraries were sequenced on Illumina NovaSeq 6000 (Illumina, San Diego, USA) using 150 bp paired-end chemistry. The data obtained from the sequencing run was de-multiplexed using Bcl2fastq2 softwarev2.20 and FastQ files were generated based on the distinct

dual barcode sequences. The sequencing quality was assessed using FastQC3 v0.11.8 software and Trimgalore- v0.4.0.

2.2.2. Nanopore Library preparation, Sequencing and preprocessing of reads

The NEBnext ultra II end repair kit was used to end polish and A-tail the genomic DNA. A blunt TA ligase master mix was used to barcode the end-prepared samples. With NEB Quick T4 DNA Ligase, sequencing adapters were ligated onto double standard DNA fragments to create the library. The prepared library was ready to use the following purification using AMPure XP beads. Qubit was used to quantify the prepared library.

The estimated DNA was combined and sequenced using a PromethION flow cell (FLO-PRO114M) on a Nanopore PromethION system (PromethION P24 and Data Acquisition Unit, ONT, Oxford, UK) following the necessary data amount and effective library concentration. Porechop-v0.2.4 was used to process the Nanopore raw reads.

2.2.3. Assembly and Annotation

The high-quality processed reads were used for d*e novo* assembly using the MaSuRCA5-v3.4.2 assembler [26]. The assembled genome was further improved by closing the gaps using LRGapcloser6-v3.0 and finally, scaffolds were constructed using the LRScaf-v1.1.12 [27]. The assembled genome was utilized for gene and protein prediction using the eukaryotic genome prediction tool, Braker-v2.1.4 gene prediction program [28]. The predicted proteins were searched against the Uniprot fungal database using DIAMOND-v0.8.29 [29]. The KAAS database was used to retrieve information from the BlastP program for functional annotation and pathways [30]. The database uses BLAST comparisons against the manually edited KEGG GENES database to offer functional annotation of genes [30]. Along with the annotation of the isolated study strain Cn, 11 more assembled sequences were also annotated by using the tool AUGUSTUS v3.4.0 [31].

2.3. Comparative genome analysis with reference genome

The assembled genome was also compared with the reference genome using two web-based resources, the Average Nucleotide Identity (ANI) calculator and D-Genies which are tools

used to quickly compare the sequences at the whole genome scale [32]. The assembled genome was validated for completeness and quality of the genome assembly using BUSCO-v5.4.2 [33]. The Mauve- v2.4.0 tool was used to compare the draft genome against the closest reference genome for the construction of multiple genomes in the presence of large-scale evolutionary events such as rearrangement and inversion [34].

2.4. Retrieval of global genome sequence data of *Cryptococcus neoformans*

The WGS of 11 isolates of *C. neoformans* were collected from the NCBI datasets (https//www.ncbi.nlm.nih.gov/datasets/) in FASTA format. The sequences were further analyzed for an evolutionary relationship, virulence, AFR and pan-genome. Due to the lack of fungal databases for virulence and AFR analysis, we have limited our comparative study to 12 isolates (n=11 isolates from NCBI datasets and n=1 hybrid sequenced genome).

2.5. Phylogenetic analysis

The phylogenetic analysis was carried out between the study strain Cn and the retrieved *C. neoformans* from the NCBI datasets. The extracted sequences from NCBI datasets include the species isolated from clinical (n=10) and environment (n=1). To investigate the phylogenetic placement based on MLST, the seven housekeeping genes *CAP59*, *GPD1*, *IGS1*, *SOD1*, *LAC1*, *URA5* and *PLB1* were used. Each genome was concatenated and the phylogenetic tree was constructed by the maximum likelihood method using MegaX software. Tree editing and annotation were performed using the interactive Tree of Life (iTOL) [35].

2.6. Virulence gene identification and comparative genomic study

The virulence-related genes (VRGs) (n=272) of *C. neoformans* were collected from the literature and DFVF (Database of Fungal Virulence Factors) database [15,16,18,36–43]. The listed gene sequences were retrieved from Uniprot and their presence in the annotated study genomes were identified using BLAST. The sequence with 99 to 100% identity was considered for the presence or absence of VRGs. The comprehensive result of the comparative virulome analysis was consolidated using iTOL.

2.7. AFR gene identification and comparative Analysis of Mutation Profiles

Similarly, the AFR genes of *C. neoformans* were collected from the literature. The AFR gene sequences were retrieved from Uniprot and their presence in the annotated genome was identified using BLAST with the query coverage and identity of 99 to 100% is considered as the presence or absence of virulence genes. Followed by, the protein mutations responsible for the antifungal resistance provided in the AFRbase database were compared with the annotated genomes of the study strains using CLUSTAL Omega. The comprehensive result of the comparative AFR analysis and mutation profiles was consolidated using iTOL.

2.8. Pan-genome analysis

The pan-genome analysis was performed using Orthovenn3 with a FASTA annotation file and GFF file produced by AUGUSTUS (genome annotation tool). The data was analyzed and visualized in Orthovenn3. The orthologous gene analysis was carried out by the OrthoFinder algorithm and the Markov clustering algorithm was used to generate the gene clusters. The evolutionary phylogenetic tree construction was made using FastTree2 by the maximum likelihood method. The gene family contraction and expansion analysis were performed using CAFE5.

3. Result

3.1. Sequencing and Assembly

The hybrid technology resulted in a total of 7.35 million reads at 116.05X coverage for Illumina sequencing and a total of 6.09 lakhs raw reads at 104.8X coverage for Nanopore sequencing. The genome sequences of the strain Cn were deposited under BioProject accession number PRJNA650119. The assembled genome was approximately 19 MB in size with 20 contigs. The quality check of the assembled genome showed 89.6% completeness.

3.2. Gene prediction and annotation

A total of 5673 predicted proteins were annotated successfully using the BRAKER tool. The gene ontology annotation categorizes the proteins into 3 groups such as biological process (14.87%), cellular components (41.75%) and molecular function (43.37%). The detailed gene ontology annotation is provided in Figure 2a. The functional annotation using KEGG pathways annotated 5963 genes which fall majorly into 6 categories, which include BRITE hierarchy

(3186 genes), metabolism (1294 genes), genetic information processing (831 genes), cellular processes (419 genes) and environmental information processing (97 genes). The genes (n=136) of unknown functions are categorized separately. The assembled genome was identified with 29 cellular pathways using the KAAS database. The top 10 functional pathways are depicted in Figure 2b.

3.3. Genome identity search of clinical Cn

The genome identity search using the ANI calculator indicated a 99.9% identity with the reference genome (H99). The same result was depicted in a whole genome analysis by MAUVE as a dot plot image and D Genies by a linear pairwise genome comparison image (figure 3a, 3b and 3c). The comparison of ITS region was shown to have 100% coverage and identity with *C. neoformans* var. *grubii* CBS8710 strain, isolated from Hodgkin's lymphoma patient from North Carolina.

3.4. Phylogenetic analysis using MLST

The 12 study genomes were analyzed for phylogeny by MLST genes using the MEGAX and visualized using iTOL. Phylogenetic analysis showed that all the South African isolates were grouped under the same single clade, whereas isolates from USA, India and Australia were grouped into another clade. The phylogenetic tree showed that the clinical and environmental isolates were indistinguishable, and the subspecies *grubii* and *neoformans* were distinguishable. The midpoint of the tree was divided into two major clades. **Clade 1**: Clinical strain (JEC21) from the USA, belonging to subspecies *neoformans.* **Clade 2**: Clinical and environmental strains belonging to subspecies *grubii*, further divided into: **Subclade 1**: Environmental strain (VNII) from the USA. **Subclade 2**: Clinical strains (Bt65, Bt81, Bt89, Bt133) from South Africa, grouped into 2 clusters. **Subclade 3**: Clinical strains from India (Cn), Australia (KBCN0140, KBCN0142, SACN00B1), USA (C23, H99), grouped into 5 clusters (Figure 4)

3.5. Virulome and comparative virulome analysis

Due to the lack of virulome profiling databases, the Virulence Related Genes (VRGs) collected from the literature and DFVF database were identified in the 12 genomes using BLAST (>99% coverage and >99% identity). From the literature and DFVF database, 272 VRGs of *C.*

neoformans were retrieved. Based on the functionality we categorized the VRGs into stress tolerance (n=164), capsular-associated (n=78), cell wall-associated (n=85), cell membrane-associated (n=24), nutrient acquisition, iron acquisition and homeostasis (n=39), host cell adhesion (n=32), host cell colonization (n=16), evasion of host immune response (n=49), biofilm-associated (n=9), protease (n=7), urease (n=1), toxin production (n=14), melanin associated (n=33), titan cell-associated (n=6) and morphogenesis related (n=13) genes. Thus, most of the genes involved in virulome analysis are multifaceted either directly or indirectly involved in more than one virulence trait. The list of genes in the study strain Cn belonging to each category is briefed in Figure 5.

In the virulome comparative study, H99 has the highest % of virulence genes with 99.26% (n=270) and the lowest in Bt133 with 82.14% (n=224). However, both are clinical isolates. The Cn strain has 97.06% (n=264) of virulence genes. Being an environmental isolate, VNII has 83.45% (n=227) virulence genes. For the comparative virulome analysis, the major VRGs polysaccharide capsule (*CAP10*, *CAP59*, *CAP60* and *CAP64*), melanin (*LAC1* and *LAC2*), thermotolerance (Hsp90 and *STU1*), cell adhesion (*ALG3*), iron acquisition (*CFT1*, *SIT1*, *CIR1* and RIM101), oxidative stress tolerance (*SOD1* and *SOD2*) and enzymes (*PLB1*, *URE1*, *YME1*, *RIM13*, *APR1*, *PIM1*, *SPP1*, *RBD1* and *APP2*) were used. The comparison revealed that these genes were found in almost all the *C. neoformans* spp. It was found that the strains Cn, H99 and JEC21 have all 24 major VRGs and could be more virulent than other strains (figure 6; table 1). The clinical strains Cn and H99-infected animal models have also proven to be highly virulent.

3.6. Resistome and Comparative Resistome Analysis

The AFR genes retrieved from the literature are examined for their presence in the study genomes using BLAST. The output significantly predicted AFR genes with >99% identity and sequence coverage. Around 78 genes were predicted and observed as factors promoting antifungal resistance. The Cn has ABC transporters (n=6 genes), Major Facilitator Superfamily (n=13), drug target genes (n=12), Inherent resistance genes (n=2), Stress regulator genes (n=2), DNA mismatch genes (n=5) and transcriptional regulator genes (n=37) contributing to AFR (figure 7).

Among the 12 strains, the Cn was found to harbor abundant AFR genes across certain classes of antifungals. Resistance to azole drugs were contributed by *ERG11, ERG24, ERG1, SRE1, AFR1, AFR2, PMR5, TUB1, SEY1, YOP1, TUB1* and *YAP1* genes. Resistance to echinocandins was contributed by *FKS1, CRM1,* and *Hsp90* genes. The gene for P4 ATPase and *CRM1* confers intrinsic resistance for echinocandins and the resistance to pyrimidine analog was conferred by the genes *FCY2, TMP1* and *FUR1*. Allylamines resistance was provided by the gene *ERG1*. Conveying that the strain Cn (n=78; 100%) has more AFR genes than other isolates. The possible reason would be that the hybrid genome has been identified to have more AFR genes than other strains. Despite being an environmental strain, the VNII has 53 AFR genes (68.83%).

Among 20 major antifungal resistance genes, 13 genes were commonly shared (100%) in all the 12 study strains. The genes *ERG11*, *ERG24*, *SEY1* and *ERG1* belonging to sterol biosynthesis provide resistance by the alteration of target protein structure, overexpression of target protein and increased activation of efflux pump. The gene for P4- ATPase and the gene *CRM1* provide inherent resistance by regulating the intracellular calcium concentration. The gene *FKS1* (β- glucan synthase; Cell wall synthesis) and Hsp90 (Heat shock protein 90; Cell wall regulation) provide resistance by alteration, under expression of the target protein and stress regulation. The genes *TMP1* and *FUR1* (Thymidylate synthase 1 and Uracil phosphoribosyltransferase 1; nucleotide biosynthesis) provide resistance by alteration and overexpression of target proteins. The gene *PMR5* (ABC transporter PMR5; ABC transporter) is the only common transporter protein that provides resistance to antifungal drugs (figure 8).

Among the 78 AFR genes, SNPs were detected in *ERG11* (lanosterol 14-α demethylase), *FKS1* (β- glucan synthase), *UXS1* (UDP- glucuronate decarboxylase 1), *FUR1* (Uracil phosphoribosyltransferase), *TUB1* (β tubulin) and *FCY2* (Cytosine permease) genes. Among them, *ERG11* was noted to have the highest number of mutations (n=9), followed by *UXS1* (n=2), *FKS1* (n=1), *FUR1* (n=1) and *FCY2* (n=1). The presence of SNPs in the 12 study strains is depicted in Figure 9; Table 2. In the *FKS1* gene, serine at the 643rd position was mutated to proline. This resulted in the conformational change in the lipid enriched molecules, as its role is to anchor the lipid molecules, and amino acid serine at 643rd position is involved in the binding site. In the *ERG11* gene phenylalanine (F) at 126th position has been changed to serine (S) and glycine at 464th position has been mutated to valine. Both these residues were not conferred to

active site binding pocket. In the *TUB1*, histidine at the 6th position was changed to glutamine, glutamic acid at 98th position was mutated to glycine and phenylalanine at 200th position was mutated to asparagine. Glycine at the 190th position was mutated to glutamic acid in the ABC transporter gene *FUR1*. In all the 12 study genomes, though the mutation was observed, none of them were conferred to the active site binding pocket which is also concurrent with our *in vitro* susceptibility test where the study clinical strain Cn showed sensitivity to fluconazole and amphotericin B [44].

3.7. Pan-genome analysis and phylogenetic analysis using orthologous genes

The pan-genome analysis aids in understanding the genome architecture of a species. The preliminary orthologous gene analysis showed the number of gene clusters, proteins and singleton genes in each genome (figure 10a, 10b and 10c). The overall read statistics of the orthologous genome analysis are provided in Table 3. In figure 11, the gene clusters and their associated proteins have been designated as core, shell, and cloud. The orthologous analysis generates two data sets, one is the upset chart where the unique orthologous cluster and proteins present in the 12 genomes are independent of one another and the second is the occurrence chart where the unique orthologous cluster and proteins are dependent on each other. The occurrence chart and upset chart visualize the presence and absence of orthologous gene clusters and protein count across the compared study genomes. The unique clusters and proteins of the study genomes are derived from upset chart were the gene clusters and proteins are not correlated and demonstrated in table 4. The unique clusters and proteins of the study genomes are derived from occurrence chart were the gene clusters and proteins are correlated were demonstrated in table 5. The occurrence chart and upset chart provided a correlation between the gene cluster and protein count. From the occurrence chart of the gene cluster, it was depicted that there were about n=4676 clusters (73.6%) containing n=57595 proteins (77.3%) present in all the study genomes (figure 12, 13, 14). The pan-genome analysis also states the 4304 single-copy clusters (single-copy orthologous clusters) across the 12 genomes. The single copy clusters were categorized into biological process-associated (96.68%), molecular function-associated (2.23%) and cellular component-associated (1.08%) gene clusters (Figure 15; Table 6). The phylogenetic tree was constructed by the maximum likelihood method using the orthologous genes (figure 16). The midpoint was divided into two clades where the strain JEC21 (*C. neoformans var. neoformans*)

was in **Clade1** and the rest in **Clade 2** occupied by the subspecies *grubii*. Clade 2 was further divided into 2 subclades where **subclade 1** has the environmental strain VNII (environmental strain) and **subclade 2** has clinical strains that was further categorized into 6 clusters. The gene expansion (gene duplication) and contraction (gene deletion) studies using the CAFE5 showed the addition of gene families (expansion) and contraction of gene families. The highest contraction of gene families was reported in the environmental strain VNII and the strains isolated from Australia showed mere stable expansion and contraction that were reported in figure 16. A pairwise heat map was generated based on the similarity of orthologous genes which shows that the strain Cn (clinical strain; sub sp. *grubii*) and VNII (environmental strain) have high similarity with JEC21 (clinical strain; sub sp. *neoformans*). The strain Bt65 (clinical strain) is similar to Bt81 (clinical strain) and Bt89 (clinical strain) is similar to Bt133 (clinical strain) (figure 17).

4. Discussion

In this study, we sequenced and assembled a genome of *C. neoformans* (Cn) collected from the Microbiology lab of Trichy Medical College, Tamil Nadu, India sourced from cryptococcal meningitis patient. Together with the already available 11 genomes of the species, we compared all 12 genomes and deciphered the phylogenics, resistome, virulome and pangenome of these cryptococcal strains. The genome size of all the study strains is 18.9 to 19.1 Mb and the GC contents ranged between 48 to 48.5%.

The ISHAM ITS barcoding helped to confirm the subspecies of the study strain Cn to be *grubii* (100% identity) which is in correlation with the constructed phylogenetic tree. The Cn study strain's subspecies identification also confirms that it is a member of the serotype A. Due to the lack of 100% matching sequences in the ISHAM database, we anticipate that the strain Cn might belong to a new ST type.

The phylogenetic tree constructed using the MLST genes and the orthologous genes shows similar results, especially on the strains from Botswana, South Africa. Except for the strain JEC21(California, USA), all the other strains belong to the same subspecies *grubii* the strains of USA, Australia and India showed diversities in the clades. The strains from Botswana, South Africa are present in the same subclade showing the convergence in their genome. Sub-Saharan Africa has been the hub for Cryptococcal infection and the Botswana belongs to the

southern part of Sub-Saharan Africa [12]. The genetic convergence is obvious in this part due to several factors such as strong selective pressures, high transmission rate, limited gene flow and host adaptation.

Our manual method of retrieving virulence genes from literature and BLAST analysis revealed the presence of 99.28% of virulence genes in H99. In various reported studies virulence nature of H99 was well demonstrated using animal models [45,46]. In addition, our recent demonstration of the disseminated cryptococcosis mice model also revealed the high virulent potency of H99. Confirming our manual method as an ideal one for virulome analysis, however, the creation of a virulome database is the need of the hour. The virulome analysis depicts the presence of stress tolerance genes, which are pleiotropic and contribute to virulence regulation. The ability of *Cryptococcus* sp., to adapt to the host environment depends on how well it can maintain metabolic homeostasis under stress. The upregulation of carbohydrate transport, lipid transport, and autophagy, indicates that there is a significant need for the uptake of nutrients and energy production after host infection and phagocytosis. The *Cryptococcus* sp. has a set of autophagy genes that are essential for sustaining cellular integrity, homeostasis and survival (stress tolerance). Some of the metabolic pathways such as the pentose phosphate pathway which has been regulated by ATP were also upregulated under nitrosative stress conditions. This serves as an example that the metabolic pathways were likely to be induced by stress conditions. A recent study demonstrated that the transcription factor CIR1 (master iron regulator) and RIM101 integrate iron homeostasis with a multifarious of other functions including pH sensing, nutrient and stress signaling pathway, virulence factor elaboration and cell wall biogenesis [15–17].

The study strains C23, Bt89, and Bt133 was found to lack the major virulence factor URE1, which serves to breach the BBB and host immune system. Except Cn, H99 and JEC21 all the other strains lack the gene *LAC1* that contributes majorly to the melanin production, biofilm production and inhibition of phagocytic uptake. This is also concurrent with our previous study, in which the Cn was found to have a dominant capsule, melanin production and biofilm formation [47].

While comparing the virulome of the study strain Cn and the reference genome (H99), *ATG12*, *ATG16*, *CHS4*, Alkaline phosphatase, *UGD1*, *APP1*, *BOS1* and *RAS2* were found to be absent in the study strain which contributes to immune evasion. While comparing the virulome of the reference strain and the environmental strain, *ATG4*, *ATG9*, *ATG12*, *ATG14*, *ATG18*,

ATG26, *CBP1*, *XPT1*, *CHS4*, *CHS6*, *CHS8*, *CDA3*, *URE1*, phosphatidic acid phosphatase, *SIP4*, *CAN1*, *FRR1*, *SHO1*, *CLN1*, *SEC61B*, *SEC16*, *LAC1*, copper transport protein 86, potassium transport protein, *PDK1*, Outer cell wall protein RRT8, Yeast cell wall synthesis Kre9/Knh1-like N-terminal domain-containing protein, TatD DNase family Scn1, *CAN2*, homoserine kinase, Homoserine O-acetyltransferase, α-amylase, Alkaline phosphatase, 2-Methylcitrate synthase, *UGD1*, RNaseIII, Inositolphosphorylceramide synthase subunit Kei1-domain-containing protein, *BIM1*, *VMA21*, *UGT1*, *BOS1*, *RUB1*, *SCH9*, *RAS2* were found to be absent in the environmental strain that has protease, urease, laccase, autophagy-related and cellular function.

All the 12 isolates showed most of the major VRGs (above 80%) to be found in their genome. The environmental factors such as ecological niches, temperature and host immune responses enhance the potential of Cryptococcal virulence. The soil and bird droppings are the nutrient-rich environment supporting growth and enhancing its virulence potential. The enhancement of virulence in nutrient-rich environments is due to the conserved cAMP/ PKA signaling pathway that plays a crucial role in nutrient sensing and aids in the regulation of virulence genes [48]. The ability of *Cryptococcus* spp. to thrive at 37 ^{o}C (normal human body temperature) is crucial for its pathogenicity. The interaction of *Cryptococcus* spp. with the host immune system is critical for its virulence as it can modulate the immune response pathways, particularly inhibiting the inflammasome pathway, which is essential for effective antifungal immunity[49]. This immunomodulatory activity helps the *Cryptococcus* spp. to survive and multiply within the macrophages, further enhancing its virulence. The *Cryptococcus* spp. ability to adapt to various ecological niches, coupled with its capacity to modulate the host immune responses, underscores the importance of environmental influences on its pathogenicity.

Even though all the strains contained the AFR genes with certain mutations, most of the mutational sites do not belong to the active site binding pocket. As additional supporting data, the *in vitro* investigation on the study strain and the reference strain (H99) demonstrated that both the strains were susceptible to amphotericin B (polyenes) and fluconazole (azole). With this knowledge, it was anticipated that a mutation that occurs outside the active site binding pocket might not be the cause of AFR. This comparative genomic study of *C. neoformans* on virulence and AFR gives insights into the potent targets for the development of novel antifungal drugs.

Approximately 70 % of Cryptococcal genomes have conserved functional elements (genes involved in signaling and metabolic pathways) that are pivotal for survival and enhanced

pathogenicity. The investigation of these conserved functional elements helps to develop more effective therapeutic strategies to combat this opportunistic pathogen.

The pan-genome analysis of the *Cryptococcus neoformans* gives various insights into the orthologous gene and protein levels. The number of gene clusters and proteins are not necessarily correlated. The strain KBCN0142 has the highest number of clusters (n=5995) and the strain Bt81 has the highest number of proteins (n=6366). This might be due to the fact of high redundancy, high similarity among the proteins, stringent clustering parameters, and the presence of paralogous genes. The presence of singleton proteins in the genomes shows that they are essential proteins that appear unique within the dataset and don't have any closely related homologs. The strain Cn has the highest number of singletons up to 136. The singleton showcases the unique protein function and evolutionary significance. The orthologous analysis performed demonstrated the intersection of gene clusters and proteins; unique clusters and unique proteins of each genome. Though there were unique clusters and unique proteins present in all the 12 study strain genomes, as represented by the upset charts of cluster count and protein, the occurrence chart where the gene clusters are correlated with the protein shows the absence of a unique cluster or protein in H99, C23, KBCN0140, KBCN0142 and SACN00B1. The single-copy clusters depict the group of orthologous genes that contains exactly one copy of a gene in the cluster of the study genome. Such clusters are exceptionally important in comparative genomics and evolutionary study as they represent the conserved genes that reduce the noise from gene duplication or loss events in the compared species. The single-copy gene clusters were categorized based on functional nature as a biological process, molecular process and cellular component. Among them, the biological process-related GO cluster contributes to a maximum of 96.69% (n=17262), molecular function contributes to about 2.23% (n=398) and finally, the cellular component contributes to about 1.08% (n=193). This shows that the biological process-related genes are more conserved across the species. Though the strain JEC21 belongs to the subspecies *neoformans* and the strain Cn belongs to sub sp. *grubii* the pairwise heat map shows high similarity between them which might be because both the subspecies were descendants of the same ancestor. The phylogenetic tree constructed with the orthologous genes was considered to show more evolutionary relatedness than the tree constructed with the housekeeping genes. The reason behind the statement is the comprehensive representation of the genome, robustness to homoplasy, reduced noise of gene duplication or gene loss and improved alignment quality.

These factors reflect the true evolutionary relationships among the species. In this study, the phylogenetic tree constructed using the MLST genes and orthologous genes are merely similar. The MLST genes show that the South African strains are categorized in a single clade whereas the Pan-genome phylogenetic tree shows that the strains from South Africa and Australia are also in convergence respective to their isolation regions. The gene expansion and contraction studies showed that there was expansion (additional gene copies have been gained in their lineage) or contraction (number of gene copies lost in the lineage) among the genomes of the strains being isolated from the same region. The strains from Australia alone showed mere stable gene expansion and contraction due to the presence of stable gene families (the gene families in the species are stable concerning other species showing no significant changes in size due to duplication or loss events) or equal evolutionary changes (either the expansion/contraction occurring uniformly/ not at all occurring across all the species being analyzed leading to unique changes in a single lineage).

5. Conclusion

In conclusion, this was the first study to report the complete genome sequence of a *Cryptococcus* sp. from India and to study comparative genomics of strains from different geographical locations worldwide. Our study revealed that phylogenetic tree construction using orthologous genes yields more accurate evolutionary relationships compared to MLST. Furthermore, virulome analysis identified a high presence of major VRGs in Cn and H99 strains, consistent with *invivo* virulence assays. Resistome analysis detected major AFR genes, but mutations were absent in the active site binding pocket, aligning with *in vitro* MIC tests. The study suggests, the need for a comprehensive study which includes, virulome analysis, active site prediction, and *invitro* tests to confirm the drug resistance in fungal species, very specifically to the strains that lack the critical antibiotics breakpoints. Pan-genome analysis showed gene expansion and contraction across strains. Genome plasticity (gene expansion and contraction) is a critical factor of *Cryptococcus neoformans* sub-sp. in its adaptability, virulence and ability to resist antifungals. Deciphering these mechanisms provides insights into this pathogen evolution and suggests potential targets for therapeutic interventions. In summary, the findings on virulome and resistome profiles shed light on the pathogenicity of different strains which is

crucial for understanding disease management. The study advocates the need for bioinformatic tools for resistome and virulome analysis.

Acknowledgment

We thank SASTRA Deemed University for providing the research facilities and infrastructure.

Disclosure statement

No potential conflict of interest was reported by the authors.

Funding

The author(s) reported there is no funding associated with the work featured in this article.

References

1. do Carmo FN, de Camargo Fenley J, Garcia MT, Rossoni RD, Junqueira JC, de Barros PP, et al. Cryptococcus spp. and Cryptococcosis: focusing on the infection in Brazil. Brazilian J Microbiol. 2022;1321–37.

2. Kwon-chung KJ, Fraser JA, Doering TL, Wang ZA, Janbon G, Idnurm A, et al. gattii , the Etiologic Agents of Cryptococcosis. Cold Spring Harb Prespectives Med. 2014;4:a019760.

3. Xess I, Pandey M, Dabas Y, Agarwal R, Das S, Srivastava PMV, et al. Multilocus Sequence Typing of Clinical Isolates of Cryptococcus from India. Mycopathologia [Internet]. 2021;186:199–211. Available from: https://doi.org/10.1007/s11046-020-00500-6

4. Casalini G, Giacomelli A, Antinori S. The WHO fungal priority pathogens list: a crucial reappraisal to review the prioritisation. The Lancet Microbe [Internet]. 2024;5:717–24. Available from: http://dx.doi.org/10.1016/S2666-5247(24)00042-9

5. Chayakulkeeree M, Perfect JR. Cryptococcosis. Infect Dis Clin North Am. 2006;20:507–44.

6. Sabiiti W, May RC. Mechanisms of infection by the human fungal pathogen. Future Microbiol. 2012;7:1297–313.

7. Coelho C, Bocca AL, Casadevall A. The Tools for Virulence of Cryptococcus neoformans. Adv. Appl. Microbiol. 2014.

8. Firacative C, Meyer W, Castañeda E. Cryptococcus neoformans and Cryptococcus gattii species complexes in latin america: A map of molecular types, genotypic diversity, and antifungal susceptibility as reported by the latin american cryptococcal study group. J Fungi. 2021;7.

9. Maziarz EK, Perfect JR. Cryptococcosis. Infect Dis Clin North Am. 2016;30:179–206.

10. Rathore SS, Sathiyamoorthy J, Lalitha C, Ramakrishnan J. A holistic review on Cryptococcus neoformans. Microb Pathog [Internet]. 2022;166:105521. Available from: https://doi.org/10.1016/j.micpath.2022.105521

11. Diniz-lima I, Marques L, Silva-junior EB, Cristina J, Freire-de-lima L, Nascimento DO, et al.

applied sciences Cryptococcus : History , Epidemiology and Immune Evasion. 2022;

12. Rajasingham R, Govender NP, Jordan A, Loyse A, Shroufi A, Denning DW, et al. Articles The global burden of HIV-associated cryptococcal infection in adults in 2020 : a modelling analysis. Lancet Infect Dis [Internet]. 2022;3099:1–8. Available from: http://dx.doi.org/10.1016/S1473-3099(22)00499-6

13. Chen Y, Shi ZW, Strickland AB, Shi M. Cryptococcus neoformans Infection in the Central Nervous System : The Battle between Host and Pathogen. 2022;

14. Snelders E, Moyrand F, Sturny-Leclère A, Vernel-Pauillac F, Volant S, Janbon G, et al. The role of glycosylphosphatidylinositol (gpi) anchored proteins in Cryptococcus neoformans. Microbes Infect. 2022;24.

15. Ding H, Caza M, Dong Y, Arif AA, Horianopoulos LC, Hu G, et al. ATG genes influence the virulence of Cryptococcus neoformans through contributions beyond core autophagy functions. Infect Immun. 2018;86:1–24.

16. Jiang ST, Chang AN, Han LT, Guo JS, Li YH, Liu TB. Autophagy Regulates Fungal Virulence and Sexual Reproduction in Cryptococcus neoformans. Front Cell Dev Biol. 2020;8.

17. Zhao X, Feng W, Zhu X, Li C, Ma X, Li X. Conserved Autophagy Pathway Contributes to Stress Tolerance and Virulence and Differentially Controls Autophagic Flux Upon Nutrient Starvation in Cryptococcus neoformans. 2019;10:1–14.

18. Brown SM, Campbell LT, Lodge JK. Cryptococcus neoformans, a fungus under stress. Curr Opin Microbiol. 2007;10:320–5.

19. Gow NAR, Johnson C, Berman J, Coste AT, Cuomo CA, Perlin DS, et al. The importance of antimicrobial resistance in medical mycology. 2022;1–12.

20. Cao C, Wang Y, Husain S, Soteropoulos P, Xue C. Echinocandin Resistance in Cryptococcus neoformans. 2019;

21. Park YD, Sun W, Salas A, Antia A, Carvajal C, Wang A, et al. Identification of multiple cryptococcal fungicidal drug targets by combined gene dosing and drug affinity responsive target

stability screening. MBio. 2016;7.

22. Alastruey-Izquierdo A, Martín-Galiano AJ. The challenges of the genome-based identification of antifungal resistance in the clinical routine. Front Microbiol. 2023;14:1–8.

23. Patiño LH, Muñoz M, Ramírez AL, Vélez N, Escandón P, Parra-Giraldo CM, et al. A Landscape of the Genomic Structure of Cryptococcus neoformans in Colombian Isolates. J Fungi. 2023;9.

24. Arastehfar A, Gabaldón T, Garcia-Rubio R, Jenks JD, Hoenigl M, Salzer HJF, et al. Drug-resistant fungi: An emerging challenge threatening our limited antifungal armamentarium. Antibiotics. 2020;9:1–29.

25. QIAseq ® FX DNA Library Kit Handbook. 2023;

26. Zimin A V, Marc G, Puiu D, Roberts M, Salzberg SL, Yorke JA. Genome analysis The MaSuRCA genome assembler. 2013;29:2669–77.

27. Xu G, Xu T, Zhu R, Wang H, Li J. LR Gapcloser : a tiling path-based gap closer that uses long reads to complete genome assembly. 2018;1–14.

28. Hoff KJ, Lomsadze A, Stanke M, Borodovsky M. BRAKER2 : automatic eukaryotic genome annotation with GeneMark-EP + and AUGUSTUS supported by a ´ s ˇ Br una Tom a. 2021;3:1–11.

29. Buchfink B, Xie C, Huson DH. Fast and sensitive protein alignment using DIAMOND. 2015;12.

30. Moriya Y, Itoh M, Okuda S, Yoshizawa AC, Kanehisa M. KAAS : an automatic genome annotation and pathway reconstruction server. 2007;35:182–5.

31. Stanke M, Morgenstern B. AUGUSTUS : a web server for gene prediction in eukaryotes that allows user-defined constraints. 2005;33:465–7.

32. Ha SYS, Lim J, Kwon S, Chun J. A large-scale evaluation of algorithms to calculate average nucleotide identity. Antonie Van Leeuwenhoek. 2017;110:1281–6.

33. Manni M, Berkeley MR, Seppey M, Zdobnov EM. BUSCO : Assessing Genomic Data Quality and Beyond. 2022;1–41.

34. Mau B, Perna NT. arXiv : 0910 . 5780v1 [q-bio . GN] 30 Oct 2009 Progressive Mauve : Multiple alignment of genomes with gene flux and rearrangement. 2014;

35. Letunic I, Bork P. Interactive Tree of Life (iTOL) v6: recent updates to the phylogenetic tree display and annotation tool. Nucleic Acids Res. 2024;78–82.

36. Azevedo R, Rizzo J, Rodrigues M. Virulence Factors as Targets for Anticryptococcal Therapy. J Fungi. 2016;2:29.

37. Lu T, Yao B, Zhang C. Original article DFVF : database of fungal virulence factors. 2012;2012:1–4.

38. Almeida F, Wolf JM. Virulence-Associated Enzymes of. 2015;

39. Zaragoza O. Basic principles of the virulence of Cryptococcus. Virulence [Internet]. 2019;10:490–501. Available from: https://doi.org/10.1080/21505594.2019.1614383

40. Malachowski AN, Yosri M, Park G, Bahn YS, He Y, Olszewski MA. Systemic approach to virulence gene network analysis for gaining new insight into cryptococcal virulence. Front Microbiol. 2016;7:1–14.

41. Zhang S, Hacham M, Panepinto J, Hu G, Shin S, Zhu X, et al. The Hsp70 member, Ssa1, acts as a DNA-binding transcriptional co-activator of laccase in Cryptococcus neoformans. Mol Microbiol. 2006;62:1090–101.

42. Verma S, Shakya VPS, Idnurm A. Exploring and exploiting the connection between mitochondria and the virulence of human pathogenic fungi. Virulence [Internet]. 2018;9:426–46. Available from: https://doi.org/10.1080/21505594.2017.1414133

43. Brandão F, Esher SK, Ost KS, Pianalto K, Nichols CB, Fernandes L, et al. HDAC genes play distinct and redundant roles in Cryptococcus neoformans virulence. Sci Rep. 2018;8:1–17.

44. Rathore SS, Isravel M, Vellaisamy S, Raj D. Exploration of Antifungal and Immunomodulatory Potentials of a Furanone Derivative to Rescue Disseminated Cryptococosis

in Mice. Sci Rep [Internet]. 2017;1–14. Available from: http://dx.doi.org/10.1038/s41598-017-15500-8

45. Bosch C, Toplis B, Van Staden ADP, Volschenk H, Smith C, Dicks L, et al. Exposure of Cryptococcus neoformans to low nitrogen levels enhances virulence. Int Microbiol. 2024;

46. Fernandes KE, Fraser JA, Carter DA. Lineages Derived from Cryptococcus neoformans Type Strain H99 Support a Link between the Capacity to Be Pleomorphic and Virulence. MBio. 2022;13.

47. Rathore SS, Raman T, Ramakrishnan J. Magnesium Ion Acts as a Signal for Capsule Induction in Cryptococcus neoformans. 2017;

48. Caza M, Kronstad JW. The cAMP/protein kinase a pathway regulates virulence and adaptation to host conditions in cryptococcus neoformans. Front Cell Infect Microbiol. 2019;9:1–15.

49. Bürgel PH, Marina CL, Saavedra PHV, Albuquerque P, De Oliveira SAM, Veloso Janior PH de H, et al. Cryptococcus neoformans Secretes Small Molecules That Inhibit IL-1 β Inflammasome-Dependent Secretion. Mediators Inflamm. 2020;2020.

List of figures

Figure 1: A flow chart on the comprehensive methodology used in the study

Figure 2: Functional annotation:(a) GO annotation by DIAMOND database: the Gene ontology of the study strain Cn and (b) Pathway analysis by KAAS database: Top 10 pathway functions of the study strain Cn

Figure 3: Genome identity search: (a) ANI Calculation of the study strain Cn and reference strain H99; (b) Dot plot comparison using D GENIES and (c) Linear genome image using MAUVE

Figure 4: Phylogenetic tree based on MLST genes: MLST phylogeny was constructed using the maximum likelihood method with MegaX. 1000 bootstrap replicates were calculated to assess robustness. The midpoint of the phylogenetic tree was divided into two major clades by the subspecies *grubii* (red line) and *neoformans* (yellow line). The tree picture represents the environmental strain and the human represents the clinical strain. The magenta colour represents the Botswana (South Africa) strains, the blue colour represents the TamilNadu (India) strain, the orange colour represents the Melbourne (Australia) strains, the violet colour represents the Tennessee (USA) strain and the red colour represents the California (USA) strains.

Figure 5: VRGs present in the study strain Cn: The chart represents the (n=264) VRGs of Cn that were categorized into stress tolerance, cell wall-associated, cell membrane-associated, capsule-associated, morphogenesis associated, cell adhesion, immune evasion, iron acquisition, protease, nutrient acquisition, copper homeostasis, host cell membrane disruption and melanin associated genes.

Figure 6: Comparative virulome analysis: The graph represents the comparative study of the major VRGs present in the (n=12) study strains. The colored region represents the presence of genes.

Figure 7: AFR genes present in the study strain Cn: The chart represents the (n=78) AFRs of the Cn that were categorized into transporter, structural, DNA mismatch, nucleic acid synthesis, stress response and transcription factors.

Figure 8: Comparative resistome analysis: The graph represents the comparative study of the major AFR genes present in the (n=12) study strains. The colored region represents the presence of genes.

Figure 9: Comparative analysis of SNPs in the AFR genes: The graph represents the comparative study of the SNPs present in the AFR genes of the (n=12) study strains. The colored region represents the presence of genes.

Figure 10: The preliminary orthologous analysis that shows the number of gene clusters (a), proteins (b) and singletons (c) present in each study strain

Figure 11: The pictorial representation of the overall orthologous clusters and proteins

Figure 12: The pictorial representation of the occurrence chart that depicts the presence of orthologous gene clusters present and shared among the 12 genomes

Figure 13: The pictorial representation of the occurrence chart that depicts the presence of overlapping gene clusters present and shared among the 12 genomes.

Figure 14: The pictorial representation of the occurrence chart that depicts the presence of proteins present and shared among the 12 genomes.

Figure 15: Single-copy gene clusters present in 12 genomes classified as cellular component genes (a), biological process gene (b) and molecular function genes (c)

Figure 16: Phylogenetic tree based on orthologous genes: Orthologous gene-based phylogeny was constructed by the maximum likelihood method with CAFE5. The midpoint of the phylogenetic tree was divided into two major clades and further delineated into many clusters of *C. neoformans.*

Figure 17: Pairwise heatmap: The intensity of the colour gradient shows the similarity between the species

List of supplementary figures:

Supplementary figure 1: Agarose gel electrophoresis of isolated cryptococcal DNA: A- represents the HIND III digested lambda ladder and B- represents the isolated DNA of Cn strain

Supplementary figure 2: Tape station profiling: Fragment size distribution analysis of the prepared library

List of tables:

Table 1: The major VRGs of *C. neoformans* study strains

Virulence genes	**Protein Name**	**Functions**
CAP 10	Capsular associated protein 10	capsule synthesis and maintanence
CAP 59	Capsular associated protein 59	capsule synthesis and maintanence, Biofilm production, GXM transport
CAP 60	Capsular associated protein 60	capsule synthesis and maintanence
CAP 64	Capsular associated protein 64	capsule synthesis and maintanence
LAC1	Laccase1	production of melanin; regulates biofilm formation; Inhibits host cell phagocytosis
LAC2	Laccase2	production of melanin; inhibits host cell phagocytosis
STU1	protein STU1	stress responses; morphogenesis; capsule regulation
Hsp90	heat shock protein 90	regulates heat shock, oxidative stress and various physiological/ environmental stress including stress of antifungal agents; regulates capsule formation, melanin production; Regulates host immune evasion
URE1	urease1	facilitates nitrogen source utilization; alkalinization of the environment; calcium carbonate production; production of biofilm
PLB1	phospholipase B1	Immune evasion; fungal cell adhesion to host cells; nutrient acquisition; regulates titan cell formation
YME1 (C361_06299	ATP dependent metalloprotease	Catalyzes mechanism that involves a metal and related to virulence (stress response)
RIM13 (C361_05602)	Zinc metalloprotease	Catalyzes mechanism that involves a metal and related to virulence (stress response)
APR1	Aspartyl protease	Involved in host immune evasion and food acquisition

(C361_03288)		
PIM1	Protease	host immune evasion by proteolysis
SPP1 (CNAG_05742)	S2P endopeptidase	host immune evasion by proteolysis
RBD1 (CNAG_04056)	Serine peptidase	fungal cell adhesion to host cell; immune evasion; nutrient acquisition
APP2 (CNAG_04009)	Aminopeptidase 2	Proteolysis; nutrient acquisition; capsule formation; immune evasion
CFT1	CFT1 protein, Cryptococcus Fe Transporter (high affinity iron uptake)	iron acquisation
SIT1	Siderophore-iron transporter Str1	Iron acquisition
CIR1	GATA type zinc finger protein asd-4	regulates iron homeostasis, capsule formation, melanin production, stress response, and host immune evasion and pathogenesis
RIM101	pH-response transcription factor pacC/RIM101	regulates genes encoding cell wall-modifying enzymes such as chitinases, glucanases, and cell wall proteins; capsule production
ALG3	Dol-P-Man:Man(5)GlcNAc(2)-PP-Dol alpha-1,3-mannosyltransferase	Maintains cell wall integrity; Fungal cell adhesion to host cell; Immune evasion; Nutrient acquisition
SOD2	Mn superoxide dismutase	Oxidative stress tolerance (Catalyzes dismutation of toxic superoxide, converting superoxide to hydrogen peroxide and oxygen and related to virulence)
SOD1	Copper zinc superoxide dismutase	Oxidative stress tolerance (Catalyzes dismutation of toxic superoxide, converting superoxide to hydrogen peroxide and oxygen and related to virulence)

Table 2: The SNPs present in AFR genes of *C. neoformans* study strains

Genes	**Residue in protein**	**Mutation detected differently than proposed in journals**
ERG11(9)		
Y145F	active site residue	-
G484S	active site residue	-
S460T	not an active site residue	-
A457V	not an active site residue	-
I99V	not an active site residue	-
Y132F	active site residue	-
K143R	not an active site residue	-
F126L	not an active site residue	F126S
G464S	not an active site residue	G464V
FKS1 (1)		
S643P	not an active site residue	-
TUB1 (3)		
H6Q	not an active site residue	H6R
E98	not an active site residue	E98G
F200	not an active site residue	F200N
UXS1 (2)		
D306G	not an active site residue	-
Y217C	not an active site residue	-
FUR1 (3)		
G190D	not an active site residue	-
G87D	not an active site residue	-

G190E	not an active site residue	-
FCY2 (1)		
A157V	not an active site residue	-

Table 3: The overall read statistics of orthologous gene

All clusters	6353
Single copy clusters	4360
All proteins	74110
All singletons	325
% of singletons	0.44%
Total	6353

Table 4: The unique orthologous cluster and proteins present in the 12 genomes- Upset table where the unique clusters and protein count are independent

Strain	Unique cluster	Unique protein
Cn	9	9
H99	89	89
JEC21	19	19
Bt65	4	4
Bt81	2	2
Bt89	1	1
Bt133	1	1
C23	88	88
VNII	6	6
KBCN0140	87	87
KBCN0142	89	89
SACN00B1	87	87
Total	**482**	**482**

Table 5: The unique orthologous cluster and proteins present in the 12 genomes- Occurrence table where the unique clusters are correlated with the protein count

S.no.	Strain name	Unique clusters	Unique proteins
1.	JEC21	19	108
2.	Cn	9	27
3.	Bt65	4	84
4.	Bt81	2	9
5.	VNII	6	17
6.	Bt133	1	2
7.	Bt89	1	2
Total		**42**	**249**

Table 6: The single copy number genes present across the 12 genomes.

(a) Biological process cluster

GO annotation number	**Count of unique input accession**	**Function**	**% contribution**
GO:0008150	1762	Biological process	18.48
GO:0008152	1576	metabolic process	16.53
GO:0044237	1114	Cellular metabolic process	11.68
GO:0009987	1037	Cellular process	10.87
GO:0043170	968	Macromolecule metabolic process	10.15
GO:0044238	783	Primary metabolic process	8.21
GO:0006807	778	Nitrogen compound metabolic process	8.16
GO:0016070	563	RNA metabolic process	5.90
GO:0065007	496	Biological regulation	5.20
GO:0046483	459	Heterocycle metabolic process	4.81
Total	**9536**	-	-

(6b) Molecular function cluster

Molecular function			
GO annotation number	**Count of unique input accession**	**Function**	**% contribution**
GO:0016787	53	Hydrolase activity	16.11
GO:0016491	50	Oxidoreductase activity	15.20
GO:0016740	38	Transferase activity	11.55
GO:0043167	38	Ion binding	11.55
GO:0003676	35	Nucleic acid binding	10.64
GO:0003674	31	Molecular function	9.42
GO:0005215	26	Transporter activity	7.90
GO:0008233	26	Peptidase activity	7.90
GO:0000166	16	Nucleotide binding	4.86
GO:0048037	16	Cofactor binding	4.86
Total	**329**	-	-

(6c) Cellular component cluster

Cellular component function			
GO annotation number	**Count of unique input accession**	**Function**	**% contribution**
GO:0016020	36	Membrane	19.56
GO:0005575	31	Cellular compartment	16.85
GO:0044464	27	Call part	14.67
GO:0005634	24	Nucleus	13.04
GO:0005622	19	Intracellular	10.33
GO:0043226	14	Organelle	7.61
GO:0043229	14	Intracellular organelle	7.61
GO:0005739	10	Mitochondrion	5.43
GO:0005576	5	Extracellular region	2.71
GO:0005794	4	Golgi apparatus	2.17
Total	**184**	-	-

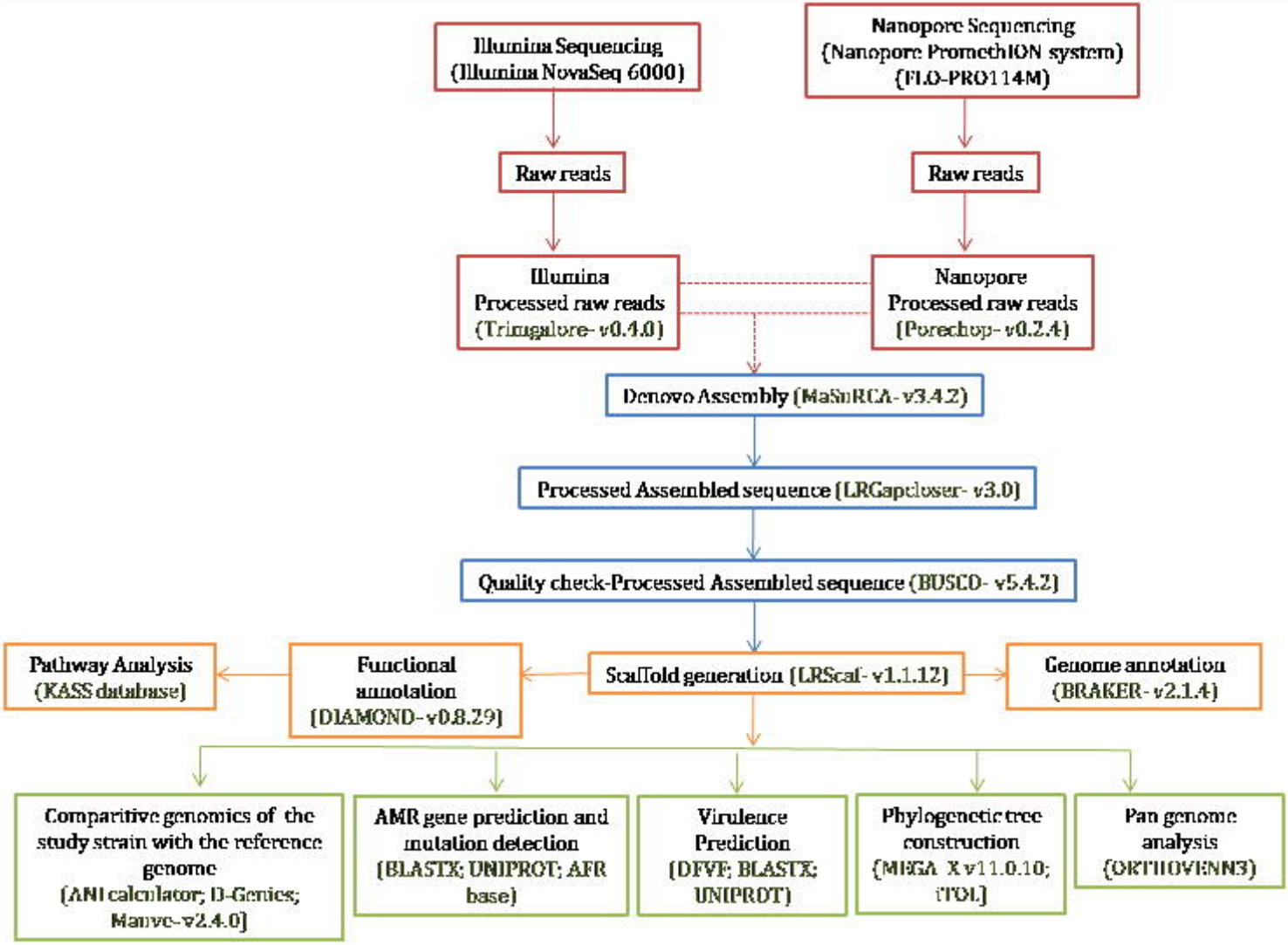
Illumina Sequencing
(Illumina NovaSeq 6000)
Nanopore Sequencing
(Nanopore PromethION system)
(FLO-PRO114M)
Raw reads
Raw reads
Illumina
Processed raw reads
(Trimgalore- v0.4.0)
Nanopore
Processed raw reads
(Porechop- v0.2.4)
Denovo Assembly (MaSuRCA- v3.4.2)
Processed Assembled sequence (LRGapcloser- v3.0)
Quality check-Processed Assembled sequence (BUSCO- v5.4.2)
Pathway Analysis
(KASS database)
Functional
annotation
(DIAMOND- v0.8.29)
ScaffOld generation (LRScaf- v1.1.12)
Genome annotation
(BRAKER- v2.1.4)
Comparitive genomics of the
study strain with the reference
genome
(ANI calculator; D-Genics;
Mauve- v2.4.0)
AMR gene prediction and
mutation detection
(BLASTX; UNIPROT; AFR
base)
Virulence
Prediction
(DFVF; BLASTX;
UNIPROT)
Phylogenetic tree
construction
(MEGA X v11.0.10;
iTOL)
Pan genome
analysis
(ORTHOVENN3)

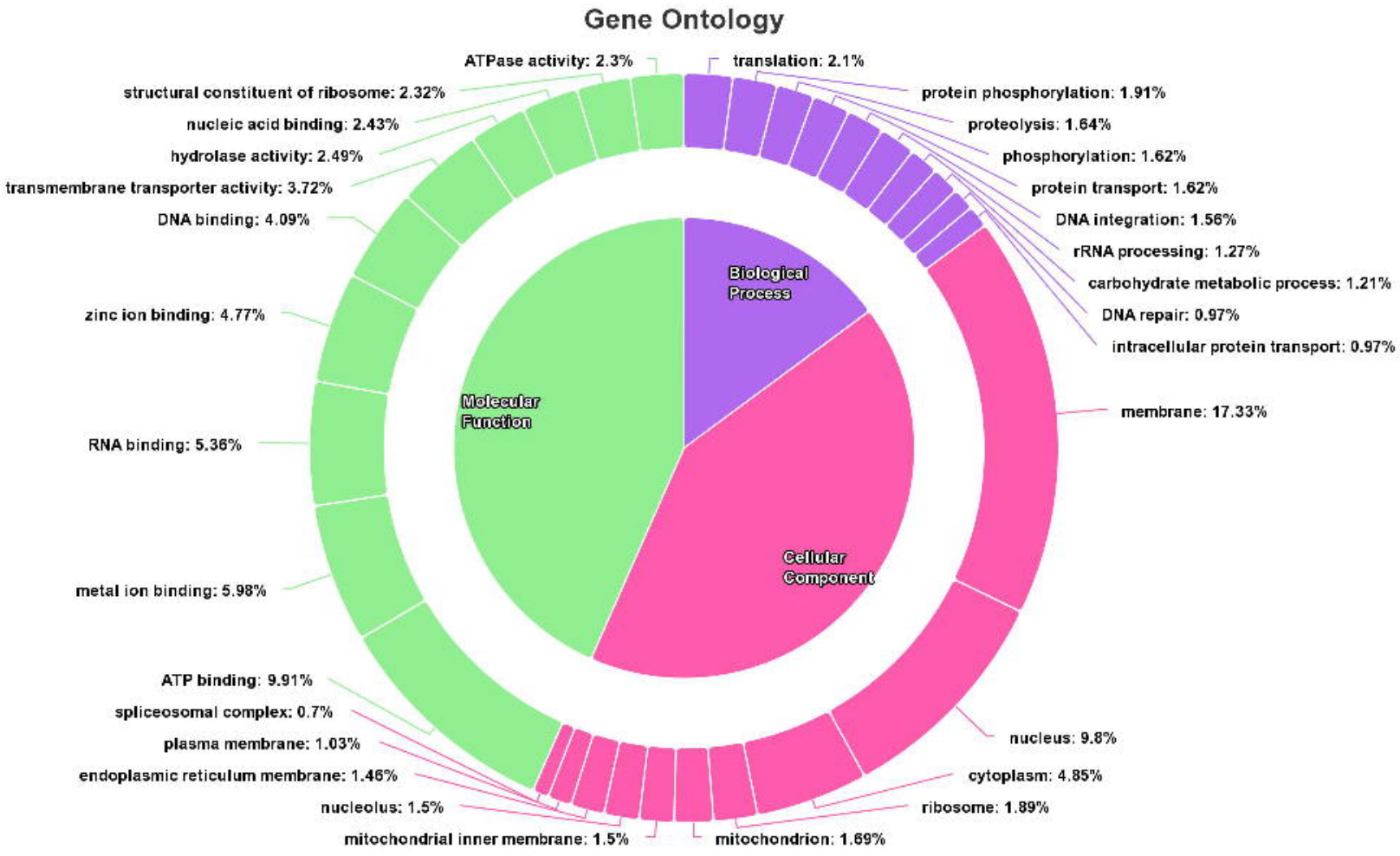
Gene Ontology
Biological Process
Molecular Function
Cellular Component
translation: 2.1%
protein phosphorylation: 1.91%
proteolysis: 1.64%
phosphorylation: 1.62%
protein transport: 1.62%
DNA integration: 1.56%
rRNA processing: 1.27%
carbohydrate metabolic process: 1.21%
DNA repair: 0.97%
intracellular protein transport: 0.97%
membrane: 17.33%
nucleus: 9.8%
cytoplasm: 4.85%
ribosome: 1.89%
mitochondrion: 1.69%
mitochondrial inner membrane: 1.5%
nucleolus: 1.5%
endoplasmic reticulum membrane: 1.46%
plasma membrane: 1.03%
spliceosomal complex: 0.7%
ATP binding: 9.91%
metal ion binding: 5.98%
RNA binding: 5.36%
zinc ion binding: 4.77%
DNA binding: 4.09%
transmembrane transporter activity: 3.72%
hydrolase activity: 2.49%
nucleic acid binding: 2.43%
structural constituent of ribosome: 2.32%
ATPase activity: 2.3%
Highcharts.com

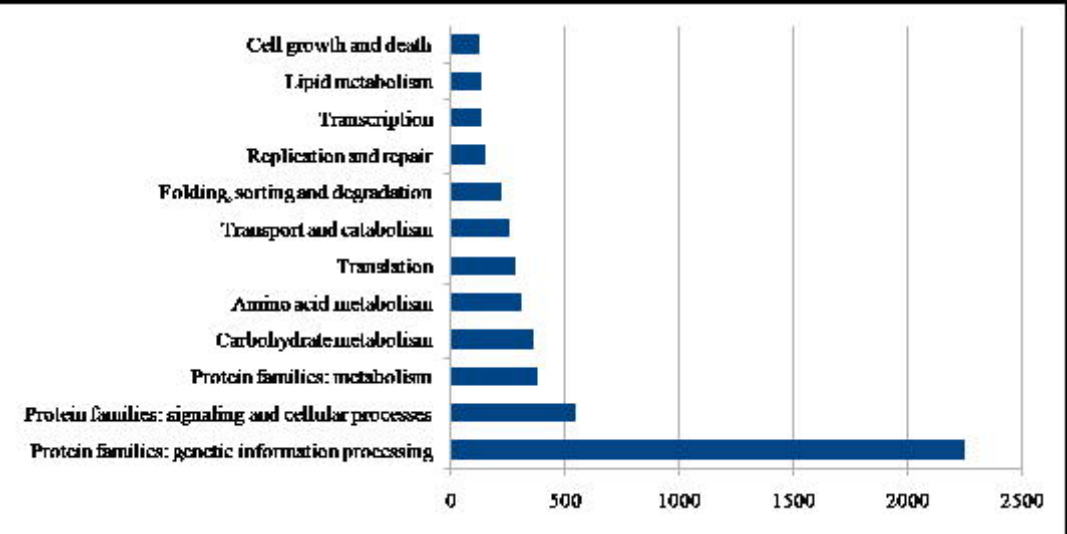
Cell growth and death
Lipid metabolism
Transcription
Replication and repair
Folding, sorting and degradation
Transport and catabolism
Translation
Amino acid metabolism
Carbohydrate metabolism
Protein families: metabolism
Protein families: signaling and cellular processes
Protein families: genetic information processing
0
500
1000
1500
2000
2500

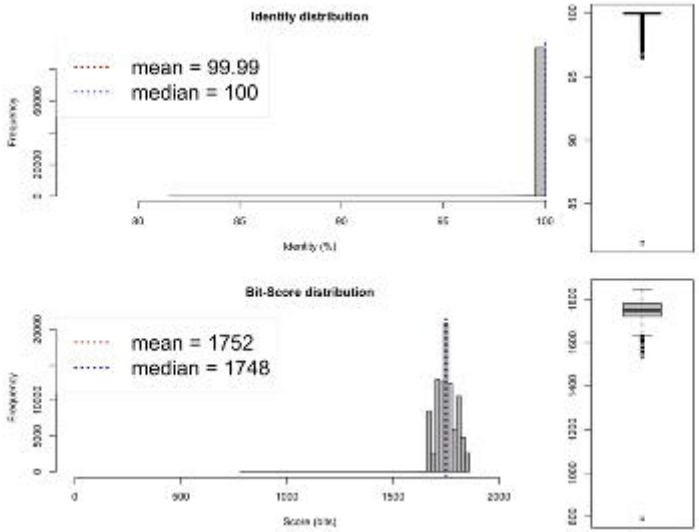
Identity distribution
mean = 99.99
median = 100
Frequency
Identity (%)
Bit-Score distribution
mean = 1752
median = 1748
Frequency
Score (bits)

(a)

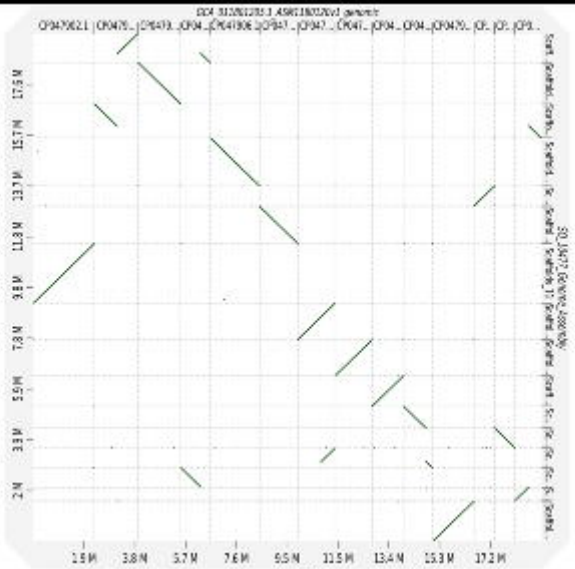

(b)

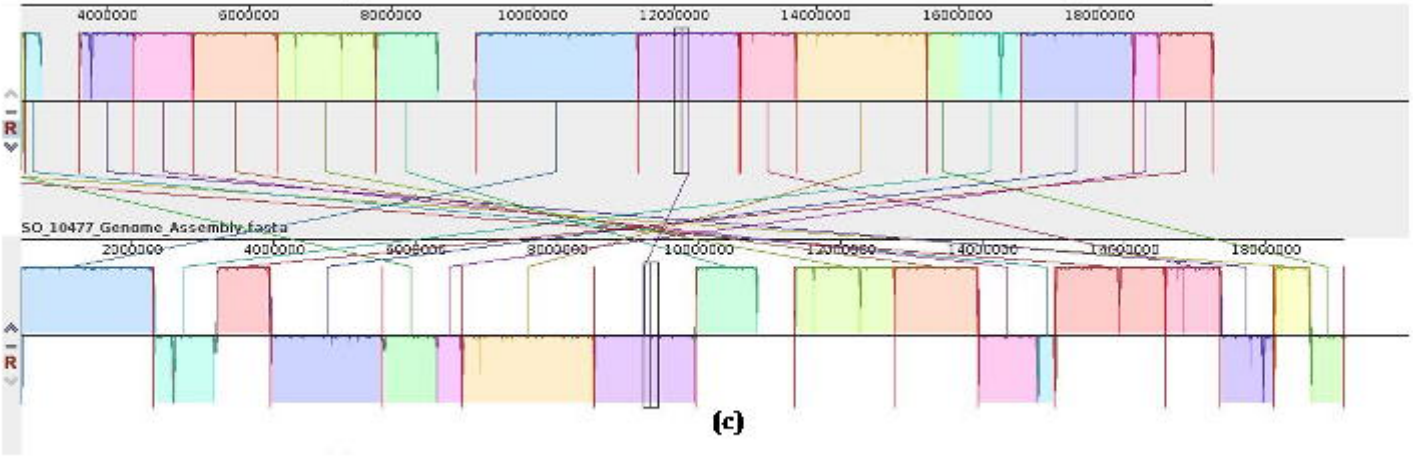
4000000
6000000
8000000
10000000
12000000
14000000
16000000
18000000
SO_10477_Genome_Assembly.fasta
2000000
4000000
6000000
8000000
10000000
12000000
14000000
16000000
18000000

(c)

VNII
Bt133
Bt89
JEC21
H99
Bt81
Bt65
SACN00B1
Cn
KBCN0140
C23
KBCN0142

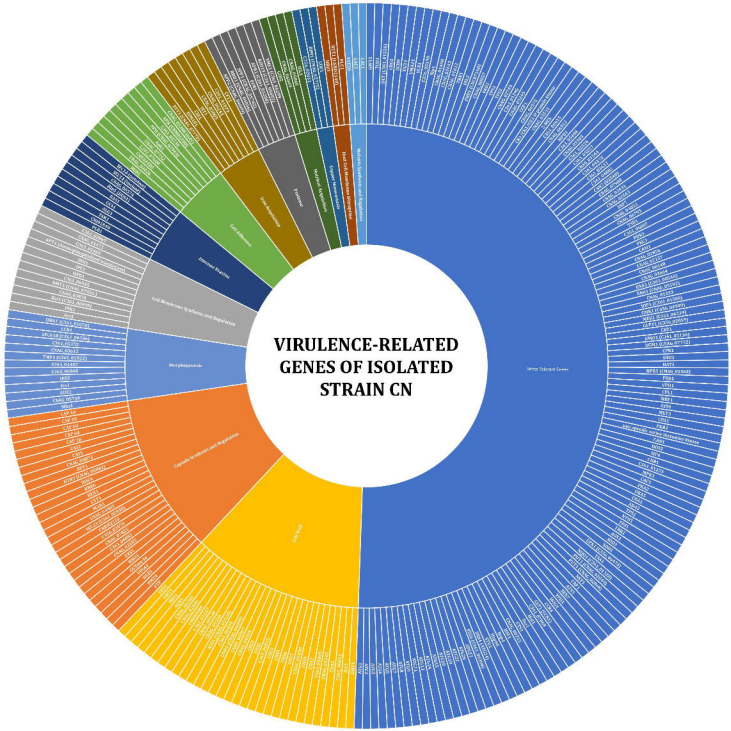
VIRULENCE-RELATED GENES OF ISOLATED STRAIN CN
Vertex Tolerant Genes
Lobes
Capsule Synthesis and Regulation
Morphogenesis
Cell Wall Synthesis and Regulation
Immune Reaction
Cell Wall Synthesis
Transfer
Nutrient Supplement
Cell Wall Synthesis and Regulation
Nutrient Supplement
Cell Wall Synthesis and Regulation
Vertex Tolerant Genes

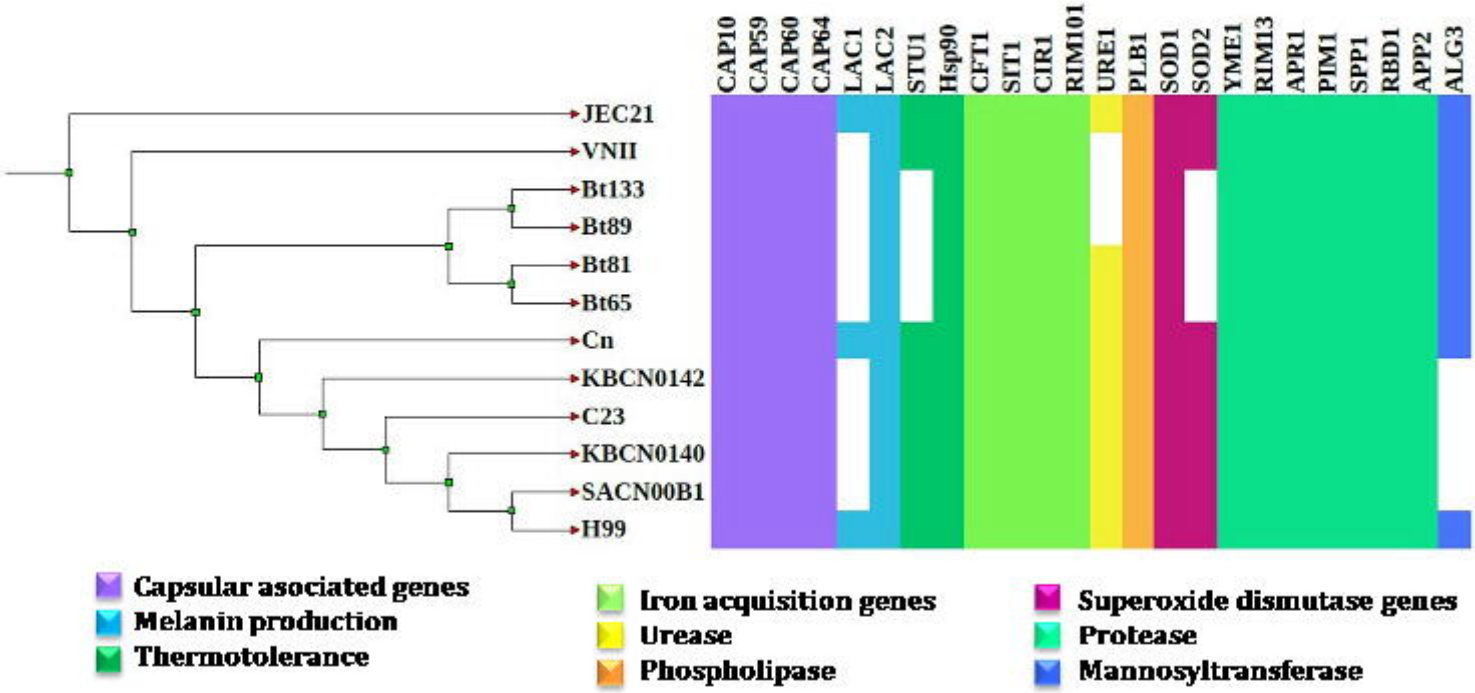
CAP10
CAP59
CAP60
CAP64
LAC1
LAC2
STU1
Hsp90
CFT1
SIT1
CIR1
RIM101
URE1
PLB1
SOD1
SOD2
YME1
RIM13
APR1
PIM1
SPP1
RBD1
APP2
ALG3
JEC21
VNII
Bt133
Bt89
Bt81
Bt65
Cn
KBCN0142
C23
KBCN0140
SACN00B1
H99
Capsular asociated genes
Melanin production
Thermotolerance
Iron acquisition genes
Urease
Phospholipase
Superoxide dismutase genes
Protease
Mannosyltransferase

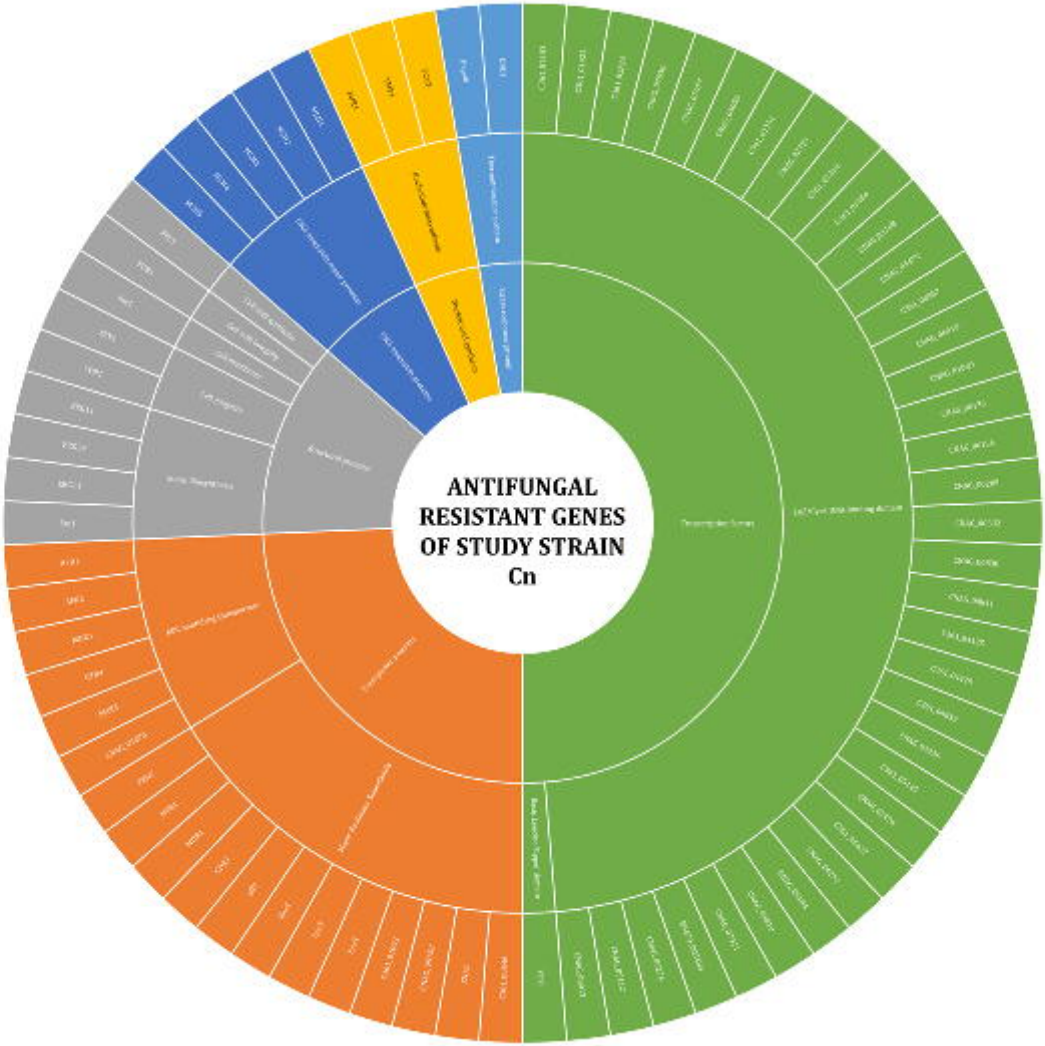
ANTIFUNGAL
RESISTANT GENES
OF STUDY STRAIN
Cn

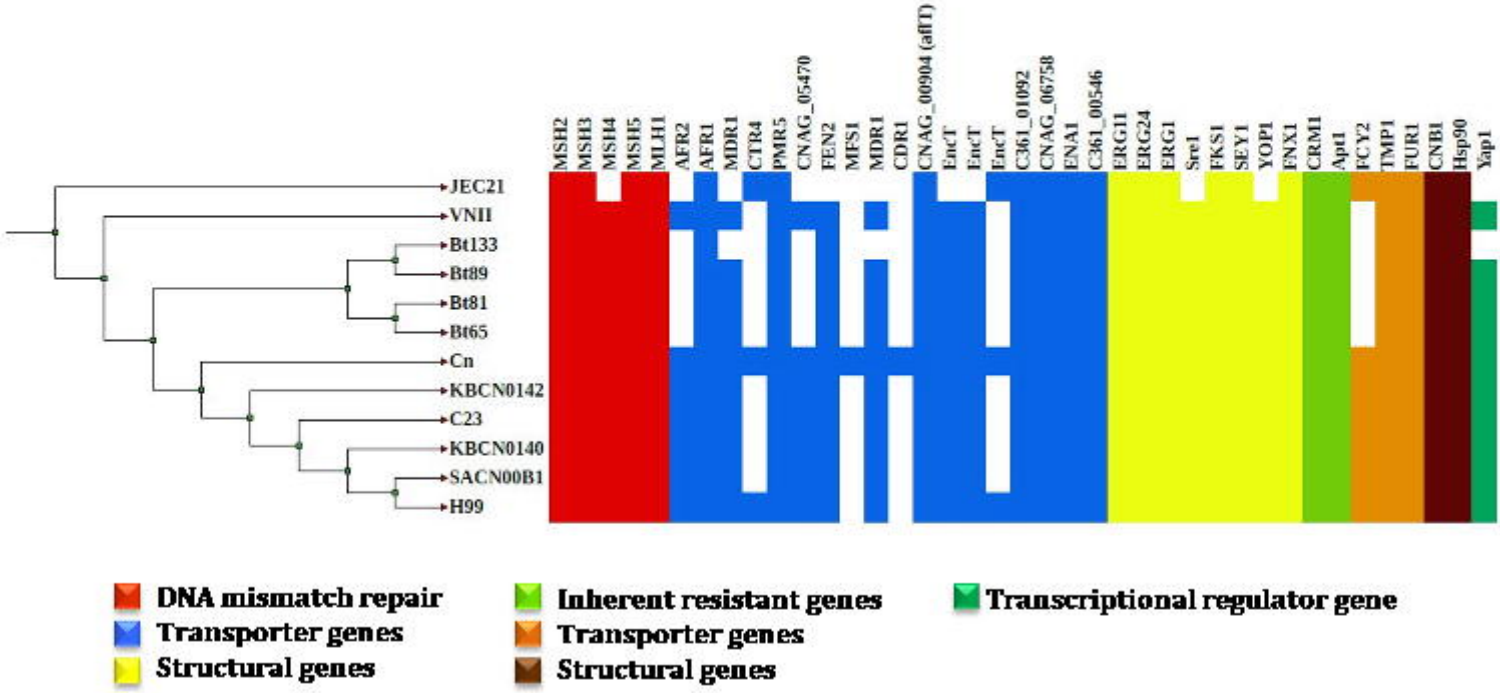
MSH2
MSH3
MSH4
MSH5
MLH1
AFR2
AFR1
MDR1
CTR4
PMR5
CNAG_05470
FEN2
MFS1
MDR1
CDR1
CNAG_00904 (affT)
EncT
EncT
EncT
C361_01092
CNAG_06758
ENA1
C361_00546
ERG11
ERG24
ERG1
Sre1
FKS1
SEY1
YOP1
FNX1
CRM1
Apt1
FCY2
TMP1
FUR1
CNB1
Hsp90
Yap1
JEC21
VNII
Bt133
Bt89
Bt81
Bt65
Cn
KBCN0142
C23
KBCN0140
SACN00B1
H99
DNA mismatch repair
Transporter genes
Structural genes
Inherent resistant genes
Transporter genes
Structural genes
Transcriptional regulator gene

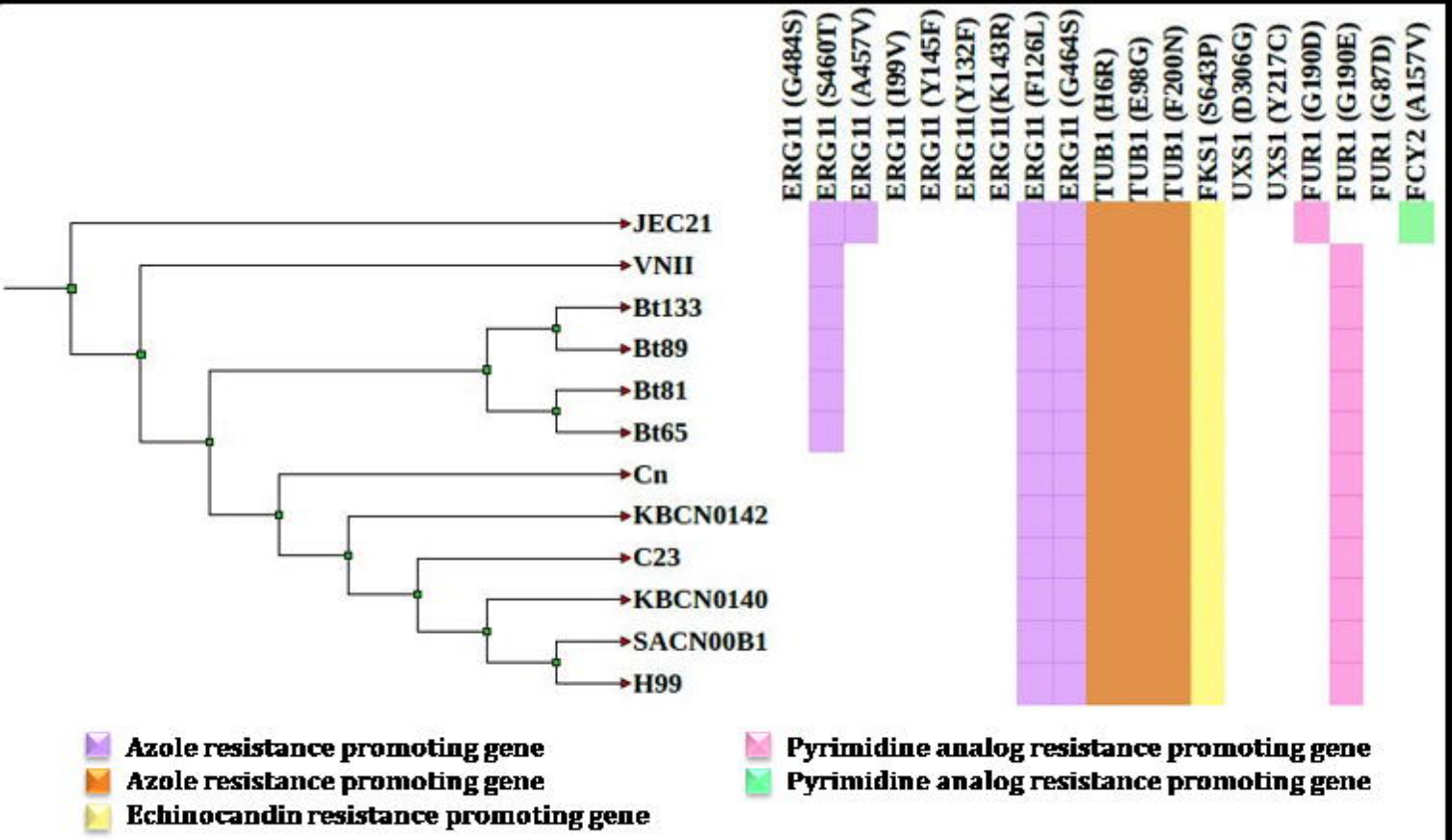
ERG11 (G484S)
ERG11 (S460T)
ERG11 (A457V)
ERG11 (I99V)
ERG11 (Y145F)
ERG11(Y132F)
ERG11(K143R)
ERG11 (F126L)
ERG11 (G464S)
TUB1 (H6R)
TUB1 (E98G)
TUB1 (F200N)
FKS1 (S643P)
UXS1 (D306G)
UXS1 (Y217C)
FUR1 (G190D)
FUR1 (G190E)
FUR1 (G87D)
FCY2 (A157V)
JEC21
VNII
Bt133
Bt89
Bt81
Bt65
Cn
KBCN0142
C23
KBCN0140
SACN00B1
H99
Azole resistance promoting gene
Azole resistance promoting gene
Echinocandin resistance promoting gene
Pyrimidine analog resistance promoting gene
Pyrimidine analog resistance promoting gene

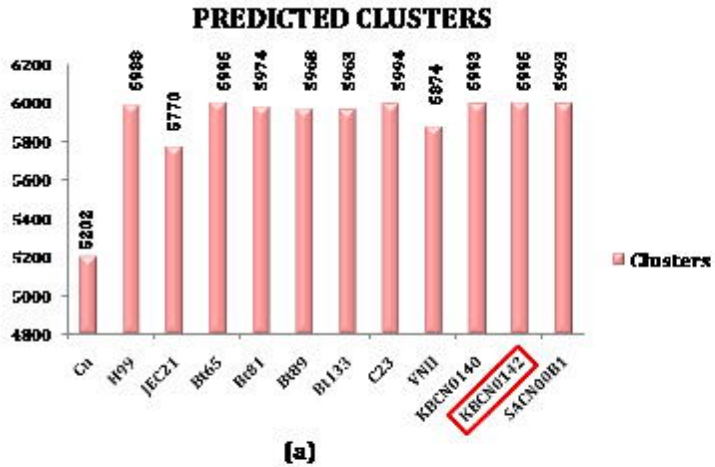
PREDICTED CLUSTERS
6200
6000
5800
5600
5400
5200
5000
4800
5202
5980
5770
5995
5974
5968
5963
5994
5874
5993
5995
5993
Ca
H99
JEC21
B65
Bt81
B89
Bt133
C23
VNII
KBCN0140
KBCN0142
SACN00B1
Clusters
(a)

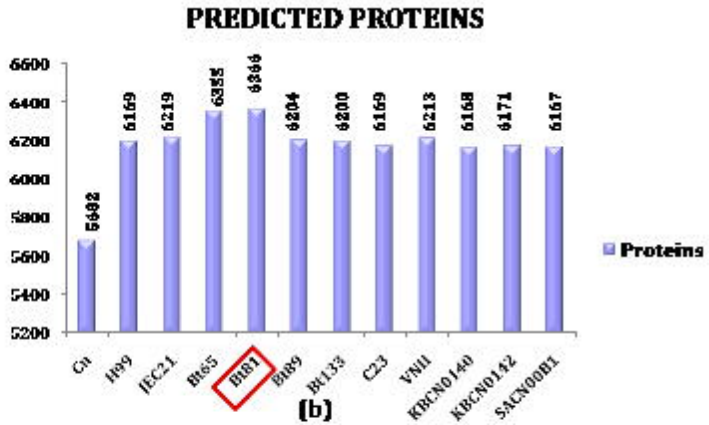
PREDICTED PROTEINS
6600
6400
6200
6000
5800
5600
5400
5200
5602
6169
6219
6355
6366
6204
6200
6169
6213
6168
6171
6167
Ca
H99
JEC21
B65
Bt81
B89
Bt133
C23
VNII
KBCN0140
KBCN0142
SACN00B1
Proteins
(b)

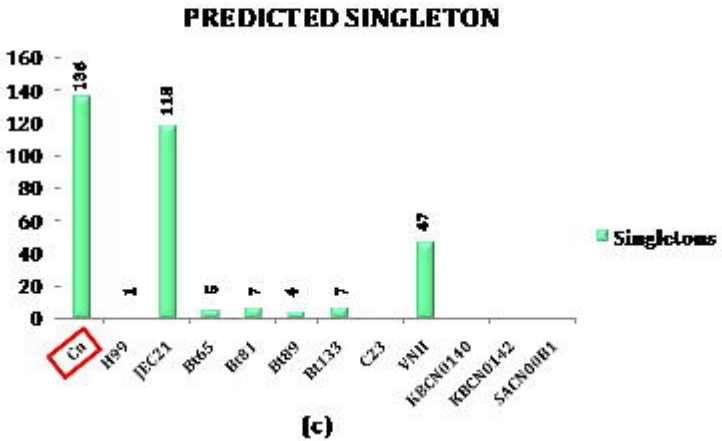
PREDICTED SINGLETON
160
140
120
100
80
60
40
20
0
136
1
118
5
7
4
7
47
Ca
H99
JEC21
B65
Bt81
B89
Bt133
C23
VNII
KBCN0140
KBCN0142
SACN00B1
Singletons
(c)

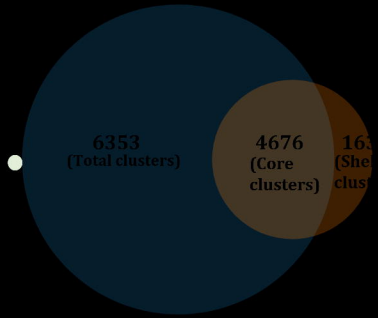
6353
(Total clusters)
4676
(Core
clusters)
16
(She
clus

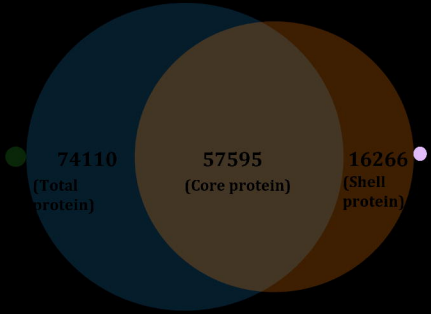
74110
(Total
protein)
57595
(Core protein)
16266
(Shell
protein)

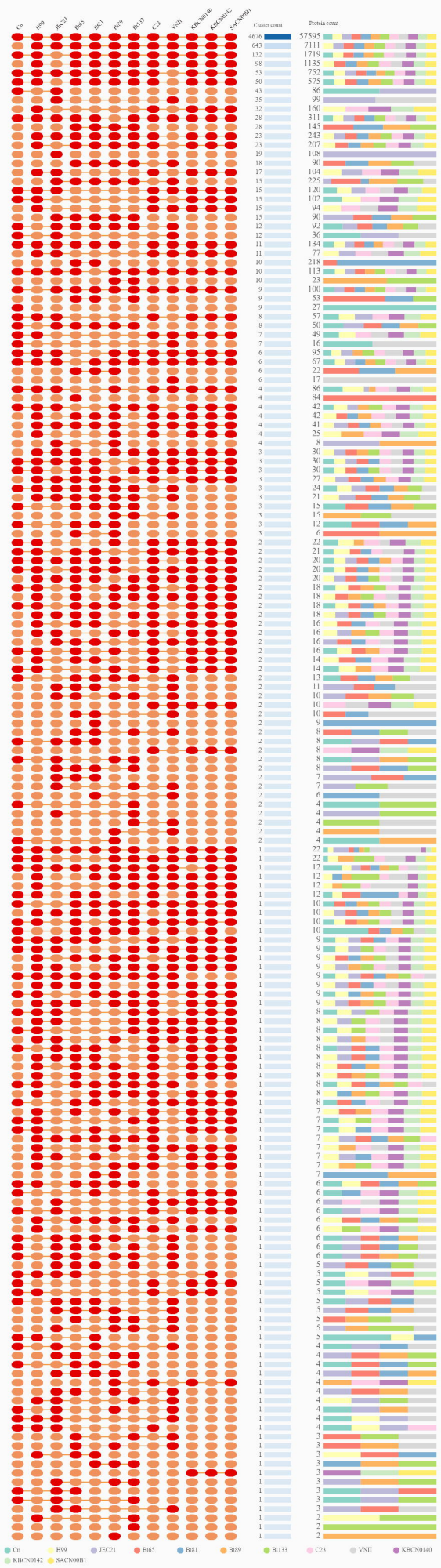
Cu
H99
JEC21
Bi65
Bi81
Bi89
Bi133
C23
VNII
KBCN0140
KBCN0142
SACN00081
Cluster count
Protein count
Cu
H99
JEC21
Bi65
Bi81
Bi89
Bi133
C23
VNII
KBCN0140
KBCN0142
SACN00081

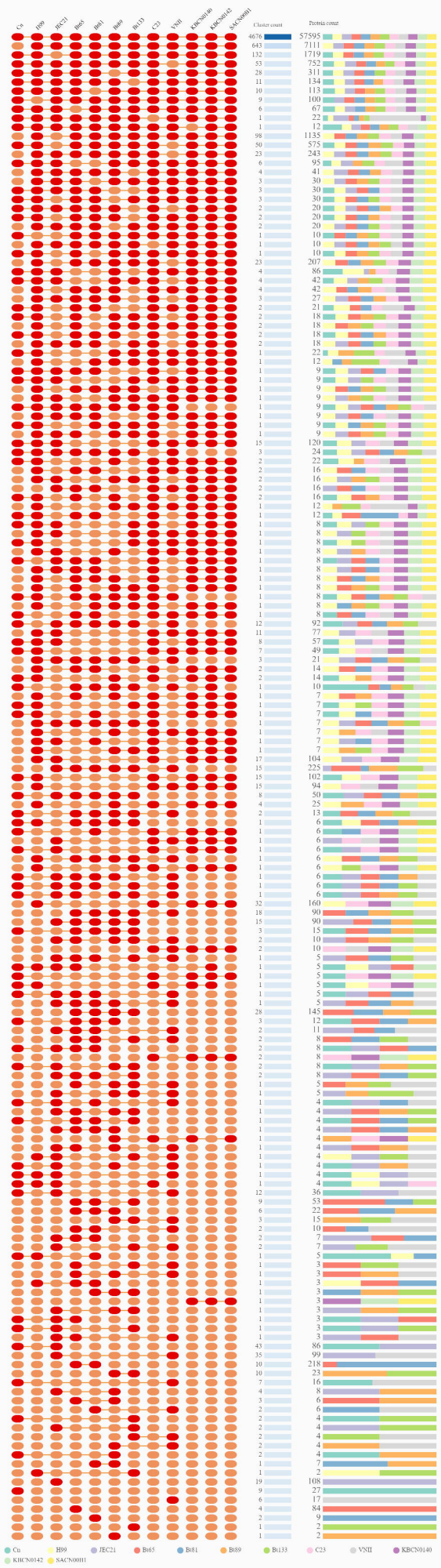
Cu
H99
JEC21
Bi65
Bi81
Bi89
Bi133
C23
VNII
KBCN0140
KBCN0142
SACN00011
Cluster count
Protein count
4676 57595
643 7111
132 1179
53 752
28 311
11 134
10 113
9 100
6 67
1 22
1 12
98 1135
50 575
23 243
6 95
4 41
3 30
3 30
3 30
2 20
2 20
2 20
1 10
1 10
1 10
23 207
4 86
4 42
4 42
3 27
2 21
2 18
2 18
2 18
2 18
1 22
1 12
1 9
1 9
1 9
1 9
1 9
1 9
1 9
15 120
3 24
2 22
2 16
2 16
2 16
1 12
1 12
1 8
1 8
1 8
1 8
1 8
1 8
1 8
1 8
1 8
1 8
12 92
11 77
8 57
7 49
3 21
2 14
2 14
1 10
1 7
1 7
1 7
1 7
1 7
1 7
17 104
15 225
15 102
15 94
8 50
4 25
2 13
1 6
1 6
1 6
1 6
1 6
1 6
1 6
1 6
1 6
32 160
18 90
15 90
3 15
2 10
2 10
1 5
1 5
1 5
1 5
1 5
1 5
28 145
3 12
2 11
2 8
2 8
2 8
2 8
2 8
1 5
1 5
1 4
1 4
1 4
1 4
1 4
1 4
1 4
1 4
1 4
1 4
1 4
12 36
9 53
6 22
3 15
2 10
2 7
2 7
1 5
1 3
1 3
1 3
1 3
1 3
1 3
1 3
1 3
1 3
43 86
35 99
10 218
10 23
7 16
4 8
3 6
2 6
2 4
2 4
2 4
2 4
2 4
1 7
1 2
19 108
9 27
6 17
4 84
2 9
1 2
1 2
Cu
H99
JEC21
Bi65
Bi81
Bi89
Bi133
C23
VNII
KBCN0140
KBCN0142
SACN00011

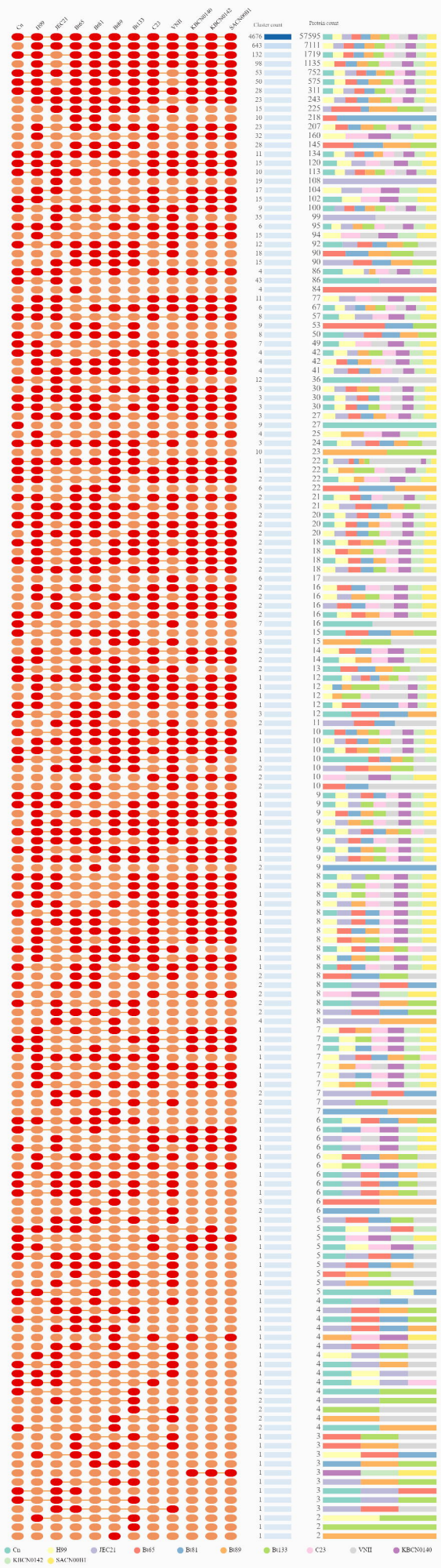
Cu
H99
JEC21
Bi65
Bi81
Bi89
Bi133
C23
VNII
KBCN0140
KBCN0142
SACN00811
Cluster count
Protein count
Cu
H99
JEC21
Bi65
Bi81
Bi89
Bi133
C23
VNII
KBCN0140
KBCN0142
SACN00811

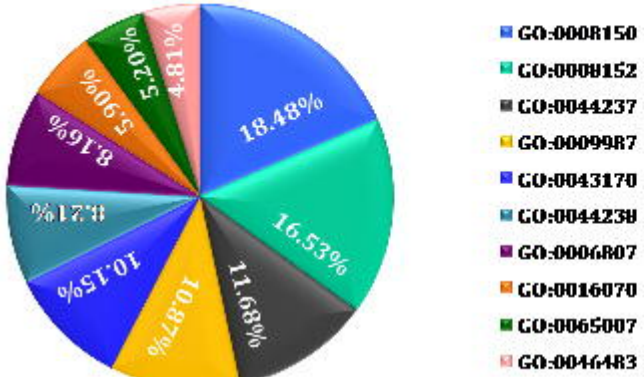
18.48%
16.53%
11.68%
10.87%
10.15%
8.21%
8.16%
5.90%
5.20%
4.81%
GO:0008150
GO:0008152
GO:0044237
GO:0009987
GO:0043170
GO:0044238
GO:0006807
GO:0016070
GO:0065007
GO:0046483

(a)

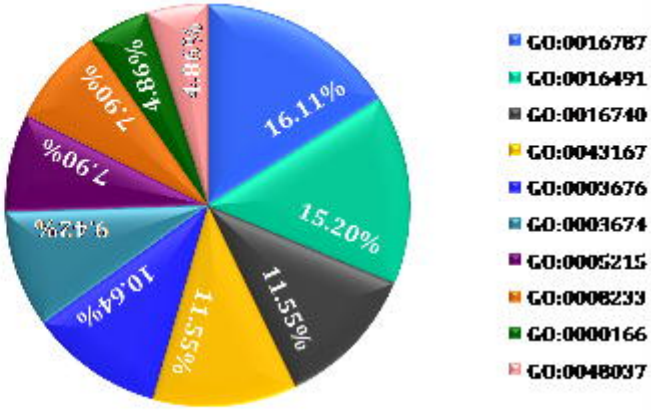
16.11%
15.20%
11.55%
11.55%
10.64%
9.42%
7.90%
7.90%
4.86%
4.86%
GO:0016787
GO:0016491
GO:0016740
GO:0043167
GO:0003676
GO:0003674
GO:0005215
GO:0008233
GO:0000166
GO:0048037

(b)

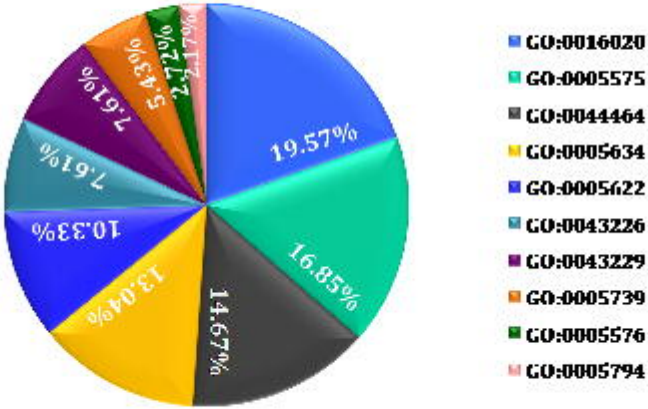
19.57%
16.85%
14.67%
13.04%
10.33%
7.61%
7.61%
5.43%
2.72%
2.17%
GO:0016020
GO:0005575
GO:0044464
GO:0005634
GO:0005622
GO:0043226
GO:0043229
GO:0005739
GO:0005576
GO:0005794

(c)

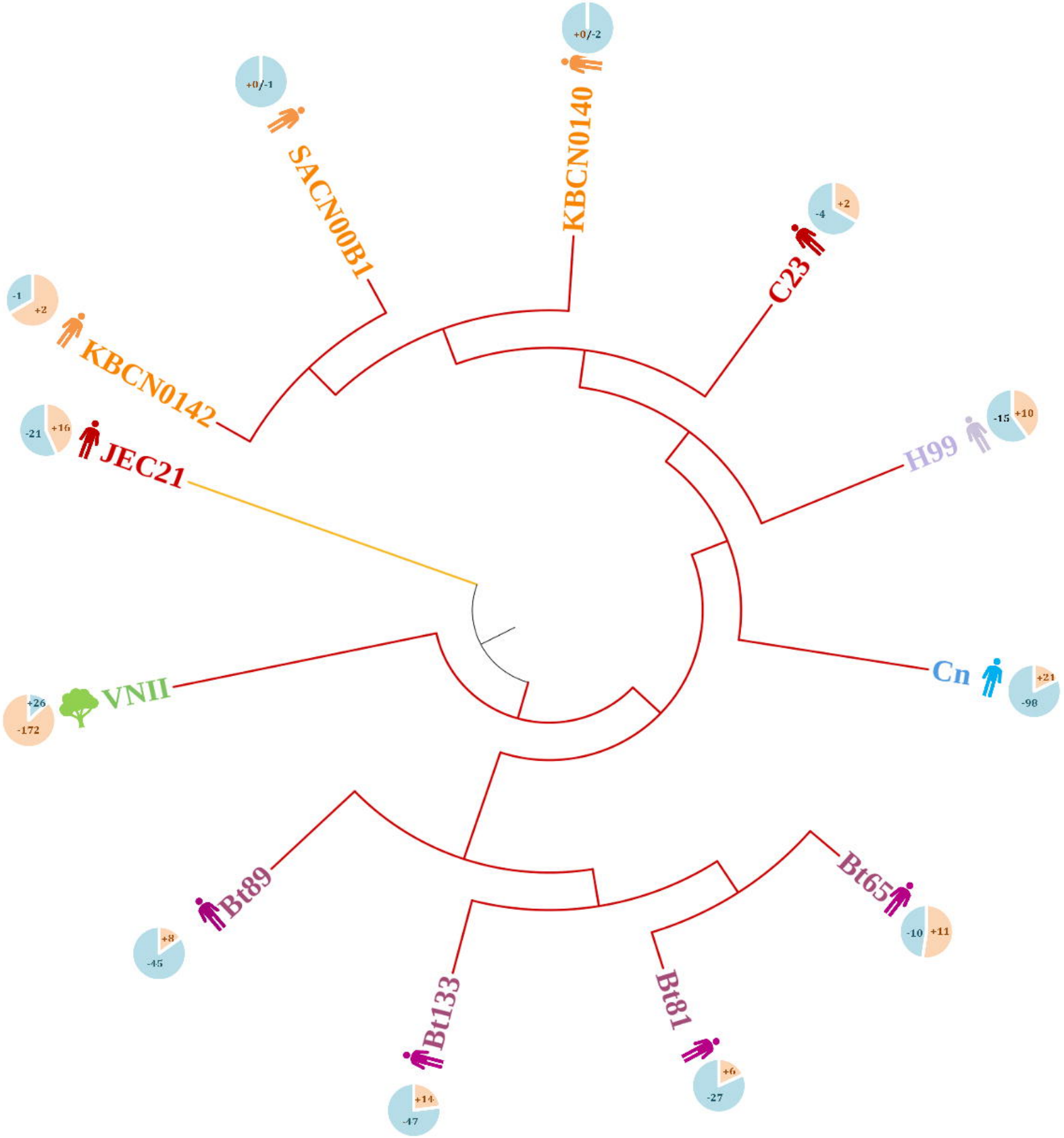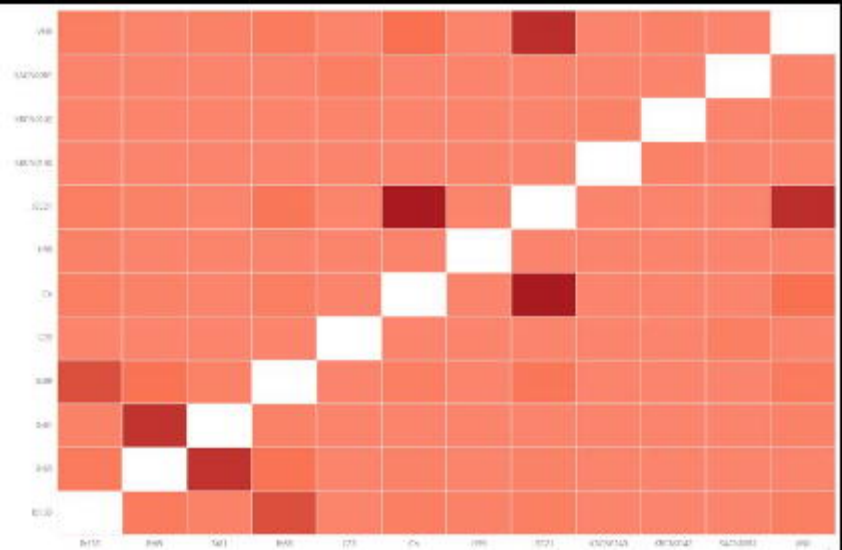
+0/-2
KBCN0140
+0/-1
SACN00B1
-4
+2
C23
-1
+2
KBCN0142
-21
+16
JEC21
-15
+10
H99
+21
-98
Cn
+26
-172
VNII
+8
-45
Bt89
Bt65
-10
+11
+14
-47
Bt133
Bt81
+6
-27